Molecular Biology of the Cell
Vol. 13, 1390–1407, April 2002

Morphology and Dynamics of the Endocytic Pathway in *Dictyostelium discoideum*[V]

Eva M. Neuhaus,* Wolfhard Almers,*† and Thierry Soldati*‡§

*Department of Molecular Cell Research, Max-Planck-Institute for Medical Research, D-69120 Heidelberg, Germany; †Vollum Institute, Portland, Oregon 97201; and ‡Department of Biological Sciences, Imperial College of Science Technology and Medicine, London SW7 2AZ, United Kingdom

Submitted August 8, 2001; Revised December 27, 2001; Accepted January 18, 2002
Monitoring Editor: Peter N. Devreotes

Dictyostelium discoideum is a genetically and biochemically tractable social amoeba belonging to the crown group of eukaryotes. It performs some of the tasks characteristic of a leukocyte such as chemotactic motility, macropinocytosis, and phagocytosis that are not performed by other model organisms or are difficult to study. *D. discoideum* is becoming a popular system to study molecular mechanisms of endocytosis, but the morphological characterization of the organelles along this pathway and the comparison with equivalent and/or different organelles in animal cells and yeasts were lagging. Herein, we used a combination of evanescent wave microscopy and electron microscopy of rapidly frozen samples to visualize primary endocytic vesicles, vesicular-tubular structures of the early and late endo-lysosomal system, such as multivesicular bodies, and the specialized secretory lysosomes. In addition, we present biochemical and morphological evidence for the existence of a micropinocytic pathway, which contributes to the uptake of membrane along side macropinocytosis, which is the major fluid phase uptake process. This complex endosomal compartment underwent continuous cycles of tubulation/vesiculation as well as homo- and heterotypic fusions, in a way reminiscent of mechanisms and structures documented in leukocytes. Finally, egestion of fluid phase from the secretory lysosomes was directly observed.

INTRODUCTION

Endocytosis is a widespread cellular function that involves the uptake of particles (phagocytosis), macromolecules, and solutes (pinocytosis) from the cell's environment via plasma membrane-derived invaginations and the subsequent digestion of ingested material.

Whereas most eukaryotic cells take up fluids for the purpose of nutrition, pinocytosis is particularly prominent in leukocytes, macrophages, and epithelial cells, where it is also involved in host defense, immunological reactions, macromolecular transport, and the regulation of metabolic pathways and signal transduction. It is remarkable that the genetic dissection of a simple eukaryote, *Saccharomyces cerevisiae*, is responsible for much of our knowledge about endocytic mechanisms (Riezman *et al.*, 1996; Geli and Riezman, 1998). Nevertheless, contrary to other eukaryotes, endocytosis is not essential for yeast survival, and despite intensive efforts, the morphology and dynamics of its endocytic pathway are still relatively obscure. It was only recently possible to produce a rough cartography of the yeast endocytic pathway at the ultrastructural level, allowing a tentative comparison with the corresponding compartments in mammalian cells (Wendland *et al.*, 1996; Hicke *et al.*, 1997; Prescianotto-Baschong and Riezman, 1998; Munn, 2001). However, due to inherent difficulties, the degree of preservation of membrane structures was poor, and it has not yet been possible to undoubtedly visualize the structure of the internalizing organelle.

D. discoideum, a social cellular amoebae that originally lived on the forest floor feeding on bacteria and yeast, has unique advantages as a model system for the investigation of endocytic processes. Laboratory strains of *D. discoideum* have pinocytosis rates 2–10-fold higher than those observed in macrophages or neutrophils (Thilo, 1985). The molecular mechanisms of membrane trafficking in the endocytic pathway of *D. discoideum* have been well investigated in recent years (reviewed in (Maniak, 1999, 2001; Neuhaus and Soldati, 1999; Rupper and Cardelli, 2001), revealing a striking degree of similarity to higher eukaryotic cells. *D. discoideum* takes up fluid mainly by macropinocytosis, a process dependent on actin, coronin, and other actin-binding proteins. Macropinocytosis was also shown to be regulated by small GTPases of the Rac family and phosphatidylinositol 3-ki-

Article published online ahead of print. Mol. Biol. Cell 10.1091/mbc.01–08–0392. Article and publication date are at www.molbiolcell.org/cgi/doi/10.1091/mbc.01–08–0392.

§ Corresponding author. E-mail address: t.soldati@ic.ac.uk.

[V] Online version of this article contains video material for some figures. Online version available at www.molbiolcell.org.

nases (reviewed in Rupper and Cardelli, 2001). Although the observed rate of formation of macropinosomes is sufficient to account for all measured fluid phase uptake (Hacker *et al.*, 1997), coated vesicles are found in *D. discoideum* and disruption of clathrin heavy chain leads to an 80% reduction in pinocytosis (O'Halloran and Anderson, 1992; Ruscetti *et al.*, 1994). Similarly to the situation in yeast (Geli and Riezman, 1998) the exact function of the clathrin molecule in uptake processes at the plasma membrane and/or later steps in the vesicle pathway is not yet elucidated. In addition, the potential contribution of different pinocytic uptake mechanisms has not been investigated. After uptake and release of the cytoskeletal coat, the fluid phase progresses through the endo-lysosomal pathway where it is rapidly acidified by delivery of proton pumps and digested by different sets of lysosomal enzymes (Souza *et al.*, 1997). Rab GTPases, clathrin, and dynamin are involved in the various vesicle-trafficking steps between the endosomes, and probably between the contractile vacuole system and the endosomes (reviewed in Maniak, 1999; Neuhaus and Soldati, 1999), but the structure of the different compartments along the endocytic pathway is largely unknown. Although very little early fluid phase recycling was observed in *D. discoideum,* endocytic trafficking is not a linear process but includes a rapid and efficient retrieval of membrane from the pinosome back to cell surface (Neuhaus and Soldati, 2000). In contrast to most higher eukaryotes, where lysosomes are often thought of as a dead end compartment, the fluid phase in *D. discoideum* is neutralized at the end of the endocytic pathway and finally egested. The nearly neutral vacuoles are again surrounded by F-actin and sequentially acquire coronin and vacuolin (Rauchenberger *et al.*, 1997; Jenne *et al.*, 1998). The exploration of membrane-trafficking mechanisms at the molecular level is being boosted by the wealth of information unveiled by the *D. discoideum* genome sequencing project, which recently culminated with a preliminary directory of >8000 predicted genes (http://dicty.sdsc.edu/annotationdicty.html).

Comparatively little work has been performed to document the morphology and dynamics of the endosomal compartments at the cellular and organellar levels. These investigations are especially relevant because adherent *D. discoideum* cells are professional phagocytes of 10–20 μm, have an overall morphology resembling that of leukocytes, are polarized cells capable of chemotactic motility, and are genetically and biochemically tractable. Previous morphological studies on *D. discoideum* have mainly focused on starvation-induced changes in the endomembrane system of the amoebae and cytochemical differences between endosomes, phagosomes, and the contractile vacuole complex (de Chastellier and Ryter, 1977; Ryter and de Chastellier, 1977; Favard-Sereno *et al.*, 1981; de Chastellier *et al.*, 1983). More recent studies showed that fluid phase markers are taken up by an actin-dependent process via crown-shaped surface protrusions that close into intracellular vesicles with an average size of 1.6 μm (Maniak *et al.*, 1995; Hacker *et al.*, 1997).

More detailed investigations of endosomal morphology have been difficult, hampering a fine structural comparison with the pathway of animal cells. Conventional aldehyde fixations result in dramatic loss of structural preservation in a very motile cell such as *D. discoideum* (Humbel and Biegelmann, 1992; Neuhaus *et al.*, 1998). In addition, the extreme dynamics of its endomembrane system together with the light sensitivity of vegetative cells severely limits the real-time morphological investigation by confocal microscopy. Herein, we present a combined light and electron microscopy (EM) study of the morphology and dynamics of the endocytic pathway in *D. discoideum.* To overcome the problems mentioned above, we used evanescent wave microscopy (total internal reflection microscopy, TIRM) for the observation of living cells and a rapid-freezing fixation to visualize the compartments at the ultrastructural level. This reveals the presence of complex tubulo-vesicular endosomes and multivesicular bodies, reminiscent of structures observed in leukocytes, which undergo continuous cycles of tubulation/vesiculation, as well as homo- and heterotypic fusions and final exocytosis. We also explored the mechanisms of fluid phase uptake and present evidence for an actin- and clathrin-independent process.

MATERIALS AND METHODS

Cell Culture

D. discoideum cells of wild-type strain AX-2 were grown in HL5c medium (Sussman, 1987) on plastic dishes at 22–23°C. Cells were plated on coverslips and allowed to adhere for several hours before investigation by light and electron microscopies.

Antibodies

The following primary antibodies were used in this study: 1) a monoclonal antibody (mAb) 176-3-6 against coronin, an actin-binding protein (de Hostos *et al.*, 1993) (gift from Dr. G. Gerisch, MPI for Biochemistry, Munich, Germany); 2) a mAb 221-342-5 (Neuhaus *et al.*, 1998) against a common mannose-6-sulfate–containing carbohydrate epitope present on *D. discoideum* lysosomal enzymes such as α-mannosidase and β-glucosidase (Knecht *et al.*, 1984; Freeze *et al.*, 1990); 3) a mAb against horseradish peroxidase (HRP) from Vector Laboratories (Burlingame, CA); 4) a polyclonal antibody against cathepsin D (gift from Dr. J. Garin; CEA, Grenoble, France); 5) a mAb 221-1-1 against vacuolin (Jenne *et al.*, 1998) (gift from Dr. M. Maniak, Abt. Zellbiologie, Universität GhK, Kassel, Germany); and 6) a mAb against a plasma membrane marker PM4C4 (mAb V4C4F3; Schwarz *et al.*, 2000) (gift from Dr. J. Garin; CEA). The secondary antibodies were either goat anti-mouse or goat anti-rabbit IgGs conjugated to cyanine 3.29-OSu (Rockland, Gilbertsville, PA) or to Alexa 488 (Molecular Probes, Eugene, OR).

Rapid Freezing of Cell Monolayers

To study the fine structure of all endocytic compartments at the EM level we fed cells with fluid phase markers that were either electron opaque or readily detectable by on-section immunostaining. The critical vitrification step needed to arrest cells in their in vivo state was done as described (Neuhaus *et al.*, 1998) by plating them on 50-μm thin sapphire coverslips (Groh+Ripp, Idar-Oberstein, Germany) and plunged into a liquid ethane slush at −175°C by using a guillotine-like device. Frozen samples were freeze substituted for 36 h in 1.5% uranyl acetate in methanol at −85°C (Monaghan and Robertson, 1990); afterward, the temperature was raised to −45°C at a rate of 5°C/h. Samples were infiltrated with Lowicryl HM-20 (Bioproducts Serva, Heidelberg, Germany) and polymerized at −45°C under UV light for 36 h. Sections of 100-nm thickness (silver/light gold interference color) were cut horizontally to the plane of the coverslip and placed onto Formvar-carbon–coated 100-mesh hexagonal copper grids. Sections were post stained for 10 min with 4% osmium tetroxide and lead citrate.

Labeling of Endocytic Compartments for EM

Cells were fed with two different fluid phase markers for investigation by EM. Colloidal gold particles of 14 nm were prepared according to Slot and Geuze (1985), and complexed with bovine serum albumin (BSA) as described (Griffiths, 1993). Alternatively, cells were fed with 10 mg/ml HRP (RZ = 3; Sigma Chemical, St. Louis, MO) in HL5c medium, and endocytosed HRP was detected after cryofixation in an on-section labeling procedure with antibodies against HRP. Lowicryl sections were preblocked for 10 min by using phosphate-buffered saline (PBS) (137 mM NaCl, 2.7 mM KCl, 8.1 mM Na_2HPO_4, 15 mM KH_2PO_4 in H_2O, pH 7.4) containing 10% fetal calf serum (FCS). After 60-min incubation with PBS/5% FCS containing the anti-HRP-antibody (1:100), the samples were washed with PBS, incubated for 60 min with rabbit anti-mouse antibody (1:100), washed in PBS, and finally incubated for 60 min with 9-nm protein A-gold (Griffiths *et al.*, 1984) diluted 1:100 in PBS/5% FCS. Grids were washed in PBS and water, air-dried, and poststained as described above. The sections were observed in a Philips 400 T transmission electron microscope (Philips, Mahwah, NJ) with an acceleration voltage of 80 kV. Kodak 4489 negatives were used and developed with Kodak D-19.

Immunofluorescence

Cells plated on grad 0 glass coverslips (80–100-μm thick; Menzel-Gläser, Braunschweig, Germany) were plunged in methanol at −85°C followed by rewarming to −35°C (by using a homemade Dewar-based temperature controlled apparatus), washing in PBS at room temperature, and incubation with PBS containing 0.2% gelatin (PBSG) for 15 min (Neuhaus *et al.*, 1998). Cells were then incubated with the primary antibodies diluted in PBSG for 30–60 min, washed in PBS, incubated for 30–60 min with fluorescently labeled secondary antibodies diluted 1:500 in PBSG, washed, and mounted in ProLong AntiFade medium (Molecular Probes). The samples were investigated with a Leica confocal microscope DM/IRB by using a 63× objective with numerical aperture 1.4. Confocal optical sections were recorded at 0.4 μm per vertical step and 8 times averaging, image stacks were imported into Adobe Photoshop (Adobe Systems, San Jose, CA) for processing.

To obtain a good rendering of cell surface morphology, fixed cells were stained with the antibody V4C4F3 directed against a plasma membrane glycoprotein, confocal sections were recorded, and projections of the resulting stacks for the whole cell were then calculated.

Evanescent Wave Microscopy

Cells were plated on coverslips and incubated with HL5c medium containing rhodamine-green dextran (Molecular Probes) at 2 mg/ml. Directly before imaging, medium containing the fluorescently labeled dextran was aspirated, cells were washed with Soerensen buffer (SB, 14.7 mM KH_2PO_4 and 2 mM Na_2HPO_4, pH 6.0) containing 120 mM sorbitol (Sigma Chemical) (SBS), flattened with a 0.2-mm-thick 2% agar sheet (Fukui *et al.*, 1987) in SBS, and imaged by evanescent field fluorescence microscopy as described using an objective specially selected for a high numerical aperture (100×, 1.4. numerical aperture; Zeiss, Welwyn Garden City, United Kingdom; Stout and Axelrod, 1989; Steyer and Almers, 1999). Fluorescence was excited with an exponentially declining, so-called evanescent field generated by total internal reflection of a 488-nm argon laser at the coverslip-cell interface. In this setup, the intensity of illumination in medium declined e-fold within ~200 nm from the coverslip, and within 640 nm in the cytoplasm of PC-12 cells (Steyer and Almers, 1999). Images were captured with a slow-scan air-cooled charge-couple device camera by using a 14-bit analog processor (ST-138S; Princeton Instruments, Trenton, NJ) and a back-illuminated imaging chip (SI502BA; Site) or with an image intensifier (VS3–1845; VideoScope International, Washington DC) and a video camera (CCDC72; Dage-MTI, Indianapolis, IN), in which case they were stored on an optical memory disk recorder (OMDR, TQ-3038F; Panasonic, Seacaucus, NJ). Images were analyzed and processed with MetaMorph (Universal Imaging, West Chester, PA), and QuickTime movies were generated using NIH Image software ((http://rsb.info.nih.gov/nih-image/).

Endocytosis

D. discoideum cells (5×10^6) were plated on 6-cm plastic Petri dishes and incubated with HL5c medium containing tetramethylrhodaminee isothiocyanate (TRITC)-dextran with molecular weight (MW) of 70,000 kDa (Sigma Chemical) at 2 mg/ml. Cytochalasin A (Sigma Chemical) in HL5c at 10 μM concentration and butanedione monoxime (Sigma Chemical) in HL5c at 50 mM concentration were added 10 min before the start of the experiment and during the uptake phase; the preincubation time was varied to exclude effects from insufficient suppression of the protein function at early time points of the experiment and no variation could be detected. For size selection experiments lucifer yellow (LY) with MW of 521 kDa and TRITC-dextran with MW of 2,000,000 kDa were diluted at 2 mg/ml and 0.5 mg/ml in HL5c. At intervals cells were rinsed from the dishes with 2 ml of ice-cold SB, 100 μl of trypan blue solution was added to quench extracellular fluorescence [2 mg/ml trypan blue (Merck Sharp and Dohme, Hoddesdon, United Kingdom) was prepared according to Hed (1986)] and samples were centrifuged for 2 min at $500 \times g$. The cell pellet was resuspended once in ice-cold SB, centrifuged, and lysed in 1 ml of SB containing 1% Triton X-100. Fluorescence intensity was measured in a SLM Aminco Bowman fluorescence spectrometer at 544-nm excitation wavelength and 574-nm emission wavelength (TRITC fluorescence) and 427-nm excitation and 535-nm emission (LY fluorescence).

RESULTS AND DISCUSSION

The major aim of this study was to exploit the synergy between high spatial resolution of transmission EM and high temporal resolution of live imaging.

Kinetics of Endocytosis and Transit in D. discoideum

We wanted to study in real time the morphology of endocytic compartments in living *D. discoideum* cells. Standard epifluorescence microscopy illuminates and records fluorescence from the whole cell. The resulting limited spatial resolution and blurring are not well suited to precise imaging of intracellular compartments (Figure 1A, epifluorescence). Confocal microscopy can image thin layers of cytoplasm but, because of light rejection by the emission pinhole, requires illumination intensities that cause rapid bleaching and phototoxicity. Most importantly, it has insufficient time resolution to visualize extremely dynamic processes. These problems were overcome by a relatively new technique, TIRM, or evanescent wave microscopy. In our setup, only a relatively thin layer of cytoplasm adjacent to the coverslip was illuminated, enabling us to follow exocytosis and plasma membrane events with high spatial and temporal resolutions (Steyer *et al.*, 1997; Steyer and Almers, 1999, 2001; Toomre *et al.*, 2000). For the first time, we show its suitability to image at video rates the fate of a fluid phase marker ingested by the cell and to directly determine the marker concentration in the endosomes as proportional to the signal intensity. In addition, directly before imaging, the cell was gently squeezed with an agar sheet overlay (Fukui *et al.*, 1987), enabling us to image roughly one-fifth of the total *D. discoideum* cytoplasm. Although it is possible to image cells with the dye around, the cells were briefly rinsed with buffer

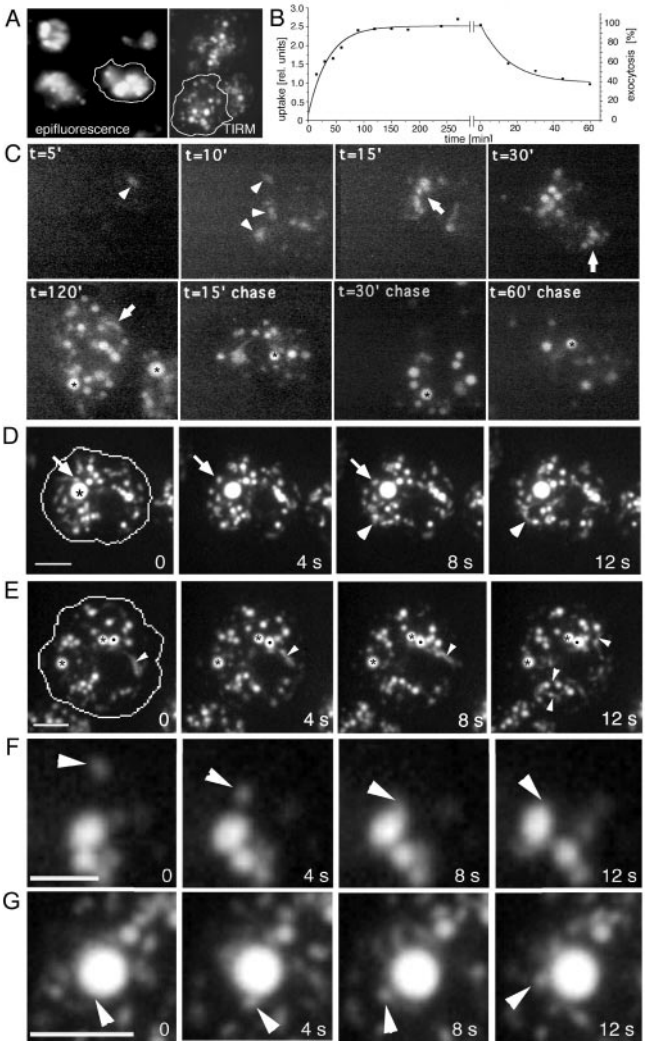

Figure 1. Endocytosis in living *D. discoideum* cells. (A) Comparison of epifluorescence microscopy and TIRM. Living *D. discoideum* cells were allowed to ingest rhodamine-green labeled dextran for 2 h, extracellular dextran was washed away to improve contrast, and endocytic compartments were visualized with both microscopes. (B) Biochemical measurements of kinetics of fluid phase uptake and egestion in wild-type *D. discoideum* cells (see MATERIALS AND METHODS). (C) Time course of fluid phase uptake and transit in wild-type *D. discoideum* cells. Cells were allowed to ingest rhodamine-green labeled dextran for different times (t = 5′ to 120′), briefly washed, and visualized by TIRM. To follow egestion, cells were fed with rhodamine-green dextran for 2 h, before incubation in dextran-free medium for the indicated times (t = 15′ chase to 60′ chase), and visualized by TIRM. Arrowheads point to dim early endosomes, arrows to small tubulo-vesicular endo-lysosomes, and asterisks highlight brighter late endosomal structures. (D–G) Endosomal morphology were studied in wild-type cells fed with rhodamine-green dextran for 3 h to ensure complete filling of all endocytic compartments and briefly washed with buffer; time-lapse series were recorded with TIRM. The cell boundaries are outlined in the first frame. (D) A big bright vacuole that was barely moving (asterisk), whereas small vesicles rapidly moved back and forth (arrow); a small group of vesicles and vacuoles that were very plastic and continuously changed shape are marked by arrowheads. The accompanying Movie 1 shows a longer time course (242 s) of the same cell. (E) Two very static vacuoles (asterisks) next to a very dynamic vacuole (dot) that continuously deformed and extended tubular structures; similar tubules extending from other vacuoles are marked by arrowheads. The accompanying Movie 2 shows a longer time course (246 s) of the same cell. Small vesicle fusing with a bigger vacuole (F); a bigger vacuole giving rise to a small vesicle (G). The movies play at 6 fps. Bars, 10 μm (C and D) and 5 μm (F and G).

before imaging to improve the contrast of the resulting picture (Figure 1A, TIRM).

Figure 1C shows *D. discoideum* cells at different time points accumulating rhodamine-green dextran, a pH-insensitive fluid phase marker. After short feeding periods, only a few labeled vacuoles, probably newly formed macropinosomes, can be seen. These have a relatively low concentration of fluid phase marker (5′ to 10′, arrowheads), which, together with their small number, gives the impression of a slow ingestion kinetics. The biochemically measured uptake kinetics of dextran-TRITC (Figure 1B) showed that *D. discoideum* cells internalized in 10–15 min one-third of the total amount reached at steady state. The apparent discrepancy between the intensity of labeling observed by microscopy and the measured amounts could be caused by illumination of only the lower one-fifth of the cell. But, because the ventral surface of *D. discoideum* is active in phagocytosis when it crawls over bacteria on a substrate, and because endosomal vacuoles in this organism are highly motile (see below), a gradient in the distribution of the endocytic compartments through the cell is unlikely. The apparent discrepancy probably results from rapid dilution of ingested dextran in a spacious unlabeled endosomal compartment, either due to repeated contacts of the macropinosome with endosomes, or due to vesicle-mediated transport of its content to stationary early endosomes. As time progresses, labeling enters most organelles of the highly heterogeneous tubulovesicular endo-lysosomal compartment, which have highest motility (arrows), until it reaches bigger, brighter endosomal vacuoles (30′ onward, asterisks). Although it is difficult to determine the degree of concentration of fluid phase marker in endosomal compartments from our fluorescence micrographs, an upper and a lower bound can be obtained as follows. First, we measured the ratio between the brightest pixels in the endosomes and the fluorescence signal in the extracellular milieu, resulting in an apparent 10–15-fold concentration. Because the dye can come closer to the coverslip beside the cell than when trapped in a cytoplasmic organelle it is illuminated with higher intensity, and thus we might underestimate the concentration in the organelles. Alternatively, we measured the ratio between the signal intensities of the dimmest and brightest endosomes, resulting in an apparent average concentration of ~50-fold. This measure might overestimate the true concentration factor as the dye is probably diluted upon arrival in a large endosomal compartment (see the argument above). It is nevertheless safe to assume that, at saturation, the dextran was concentrated 10–50-fold in some of the larger vacuoles. It is known, that during progression of ingested fluid phase through the endo-lysosomal pathway marker concentration mainly occurs at the end of the pathway, and reaches its maximum in nearly neutral vacuoles that egest indigestible remnants and lysosomal enzymes into the extracellular space (Maniak, 2001). The big bright vacuoles are the last endosomal com-

partments through which fluid phase travels and have been named postlysosomes. From now on, we will refer to them as secretory lysosomes, because they derive from lysosomes and exhibit profound similarities with some secretory organelles in mammalian cells, such as exocytic granules, that share characteristics with lysosomes (Griffiths, 1996). In addition they may contain exosomes, small membrane vesicles that are secreted by a multitude of cell types as a consequence of fusion of multivesicular late endosomes/lysosomes with the plasma membrane (Denzer *et al.*, 2000). After a chase in dextran-free medium, the labeling disappeared first from the smaller dimmer tubulo-vesicular endo-lysosomes, and later from the larger, brighter secretory lysosomes. Interestingly, the brightness of these secretory lysosomes did not change much, but their overall number decreased with time (Figure 1C, chase). Overall, these data confirm the linearity of fluid phase transit in *D. discoideum* (Aubry *et al.*, 1997; Maniak, 1999, 2001).

Real-Time Morphology of Endocytic Compartments

As can be seen in Figure 1, D and E (and in the accompanying Movies 1 and 2, sequences of wild-type *D. discoideum* cells that ingested rhodamine-green dextran for 2 h), the endosomes are extremely heterogeneous in size, shape, and movement. In contrast to a big, barely moving, intensely labeled vacuole, which probably represents a secretory lysosome (Figure 1D, asterisk), many smaller vacuoles and vesicles were found to move very rapidly through large distances (Figure 1D, and movies). Other endocytic compartments consisted of very plastic groups of vesicles and small vacuoles that constantly changed shape and extended prominent tubular structures (Figure 1D, arrowhead). Small endocytic vesicles moved around the big central vacuole but did not fuse upon every contact (Figure 1D, arrow).

Prominent tubular structures that extended repeatedly from vacuoles are marked by arrowheads (Figure 1E, black dot, and accompanying Movie 2). The very dynamic compartments were in continuous contact with other pinosomes, appeared to fuse with small vesicles (Figure 1F, arrowheads) and to give rise to vesicles (Figure 1G, arrowheads). In contrast with the latter very dynamic compartments, other vacuoles with similar morphologies were much more static (Figure 1E, asterisks), but also fused with small dextran-filled vesicles.

Ultrastructure of Endocytic Compartments

To visualize the ultrastructure of distinct organelles along the endocytic pathway of *D. discoideum* we had to solve two problems, namely, the preservation of fine structure during fixation and the use of adequate fluid phase markers. Unfortunately, it is almost impossible to avoid fixation-induced changes of the cell's living state during the aldehyde treatment included in most classical EM protocols. Membrane artifacts are often observed (Baker, 1968; Hasty and Hay, 1978; Bereiter-Hahn and Voeth, 1979), and especially tubular structures have a tendency to vesiculate, such as the lysosomal network in macrophages (Swanson *et al.*, 1987) and tubules of the contractile vacuole in *D. discoideum* (Zhu and Clarke, 1992; Fok *et al.*, 1993). We recently established a simple rapid-freezing procedure, which cryo-immobilizes the samples in the millisecond range, followed by freeze substitution and low-temperature embedding (Neuhaus *et al.*, 1998). Delicate membranous organelles such as tubular and network-like structures are well preserved by this procedure as illustrated by numerous oval, tubular, and complexly shaped structures in the sections (Neuhaus *et al.*, 1998; Figure 2).

To label endocytic compartments we used either 14-nm colloidal gold particles coated with BSA or HRP as endocytic fluid phase markers (Griffiths *et al.*, 1989). The BSA-coated gold particles (BSA-Au) are big enough to be seen directly by transmission EM without further enhancement procedures. Because HRP cannot be directly detected by the deposition of an electron-dense diaminobenzidine reaction product in freeze-substituted cells, we used an on-section labeling approach with anti-HRP antibodies.

Figure 2, A–C, shows endosomal profiles of wild-type *D. discoideum* cells that endocytosed BSA-Au. From as early as 5 min after the onset of internalization, electron-lucent vesicles containing BSA-Au and diverse tubules and vacuoles were found at the cell periphery (Figure 2A, arrowheads) as well as deeper in the cytoplasm, in the vicinity of the microtubule organizing center (our unpublished data). This contrasts with recent observations in yeast, where early endosomes were only localized at the cell periphery (Prescianotto-Baschong and Riezman, 1998) and may somehow be a consequence of the high motility of *D. discoideum* cells. Early endosomes in mammalian cells are often localized at the cell periphery, but the distribution is strongly dependent on the cell type (Geuze *et al.*, 1983; Marsh *et al.*, 1986; Gruenberg and Howell, 1987; Mellman, 1996). After a brief 5-min internalization, vacuoles filled with darker, more electron-dense material (due to higher concentrations of proteins in their lumen) were not labeled by BSA-Au (Figure 2A, asterisks). Interestingly, the morphology of electron-lucent compartments containing BSA-Au was extremely heterogeneous (Figure 2, A–C). The organelles had very different sizes, from below 100 nm up to several micrometers, some were round and some more ovals, some were shaped like "horseshoes" (Figure 2A). Many vacuoles seemed to be in tight contact with each other (Figure 2, A and B, arrows).

After prolonged internalization times other kinds of labeled structures were observed. Cells allowed to internalize BSA-Au to steady state showed large aggregates of gold particles in endosomal compartments with dark, electron-dense lumen (Figure 2, B and C). The size of the aggregate can be used as a manifestation of different stages of maturation, because clumping results from digestion by lysosomal enzymes of the protein coat on the dispersed gold particles (Bright *et al.*, 1997). Note that the "darkness" of the endosomal lumen varied somewhat between experiments. With 600–800 nm in average, the electron-dense vacuoles were slightly smaller than the early endosomal compartments but were also distributed throughout the cell. In many mammalian cells and in yeast (Prescianotto-Baschong and Riezman, 1998), late endosomal vacuoles are actually bigger than early endosomes. In addition, micrometer-long tubular structures with electron-dense lumen (Figure 2C, a 3-μm-long example) were reminiscent of the tubular lysosomes described in macrophages (Swanson *et al.*, 1987).

Figure 2F shows big, HRP-labeled early endosomes with similar, but not identical lumenal electron densities (arrowheads). Labeling was also detected in vesicular structures

near the nucleus and in the vicinity of the plasma membrane (Figure 2F, PM). Dark, electron-dense vacuoles were not labeled by anti-HRP antibodies after 5 min of internalization, but after 30 min it was common (Figure 2G, white asterisks). Some labeled vacuoles were surrounded by smaller, denser vesicular structures (Figure 2G) that might derive from the biosynthetic pathway or from storage lysosomes and participate in the early delivery of lysosomal enzymes, as, for example, *D. discoideum* cathepsin D is found in endosomes already 30 s after internalization (Journet *et al.*, 1999).

After internalization for 30 min, labeled endocytic vacuoles had varying densities. In Figure 2G (arrowheads) a big translucent vacuole sparsely labeled with antibodies and three smaller (1.3–0.5 μm), more heavily labeled vacuoles are shown. A more electron-dense lysosomal vesicle probably fuses with the vacuole in the middle. Other vacuolar or vesicular compartments belonging to the endo-lysosomal system contained single gold particles, whereas nonendosomal organelles, e.g., mitochondria (M) and the nucleus (N), were not labeled by the antibodies (Figure 2, F and G).

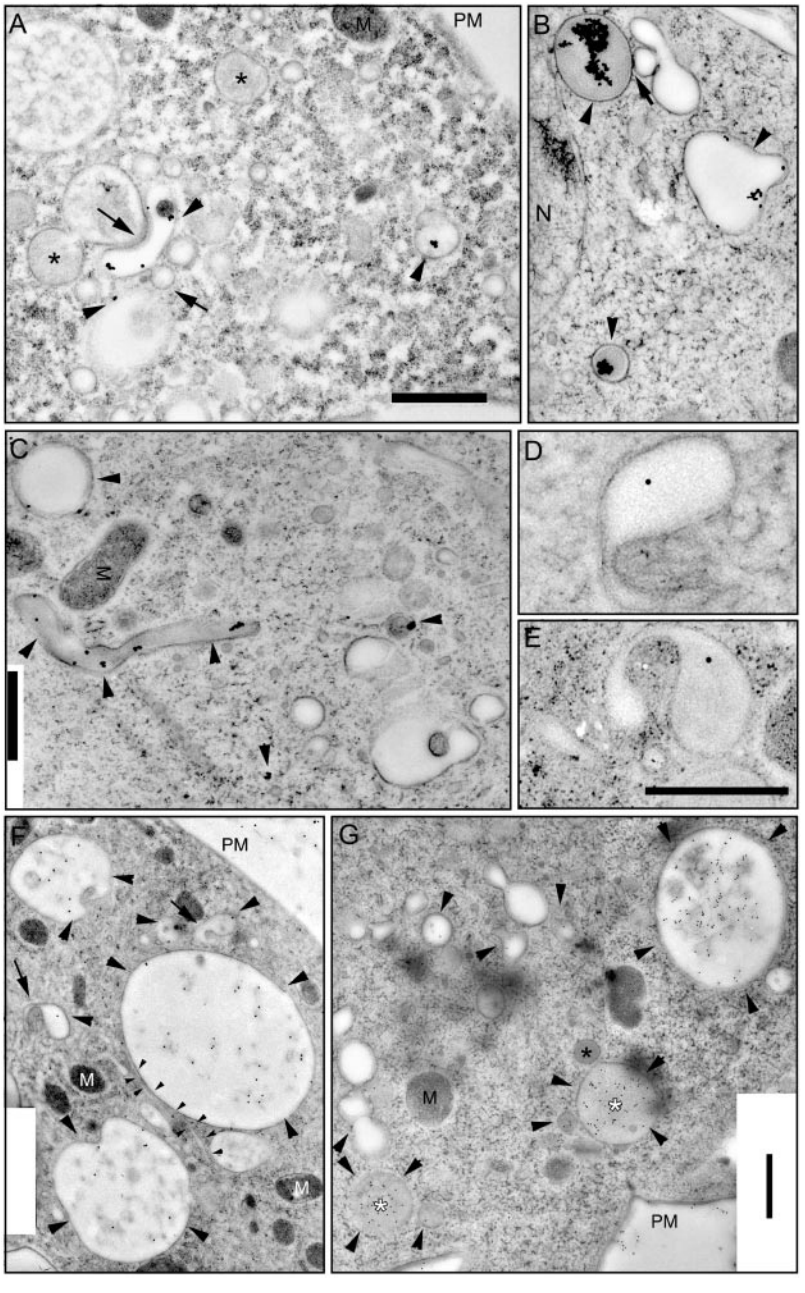

Figure 2. Ultrastructure of early and late endocytic compartments. Wild-type cells were fed with BSA-Au for 5 min (A) or 60 min (B and C) and rapidly frozen in liquid ethane. After freeze substitution and low-temperature embedding, cells were observed by EM. Arrowheads point toward compartments with internalized gold particles, and arrows point toward contact sites between endosomal vacuoles. Alternatively, cells were fed with HRP for 5 min (D–F) or 30 min (G) and rapidly frozen in liquid ethane. After freeze substitution and low-temperature embedding, endocytosed HRP was visualized on-section with anti-HRP antibodies and protein A-gold. Big arrowheads point toward vacuoles and vesicles with internalized HRP, arrows point toward tubular extensions from endocytic vacuoles. Small arrowheads in F label a long tubular structure extending from a large endosome. Black asterisks and white asterisks point to unlabeled and labeled electron-dense vacuoles, respectively. M, mitochondria; N, nucleus; PM, plasma membrane. Bars, 1 μm (A–C), 0.5 μm (D and E), and 1 μm (F and G).

Tubular endocytic structure were also revealed by this technique and had variable diameters between 50 and 200 nm, as illustrated by the long, thin (70-nm-diameter) tubule in tight contact with an endocytic vacuole shown in Figure 2F (small arrowheads). Endosomal tubules with similar sizes (30–50 nm in diameter) were also found in several mammalian cell lines, including AtT20, PC-12, HeLa, Hep2, Vero, Madin-Darby canine kidney I and II, CCL64, RK13, and normal rat kidney (Hopkins *et al.*, 1990; Tooze and Hollinshead, 1991). In addition, endosomes that seem either to extend tubules or to be in the process of invaginating membranes are shown in Figure 2F (arrows) and at higher magnification in Figure 2, D and E. Due to differences in the surface-to-volume ratios of the vacuolar and tubular parts, these endosomes could be responsible for the proposed early sorting of membranes from fluid phase (Neuhaus and Soldati, 2000).

The correlation between investigations by rapid freezing and electron microscopy with observations of living cells by TIRM revealed new facets of the overall morphology and dynamics of the endocytic pathway in *D. discoideum.* We then put to use this synergy to dissect in detail the mechanisms of fluid phase uptake, to investigate the motility of endosomes, the morphology of distinct endocytic compartments, such as multivesicular bodies, the clustering of endocytic vesicles, and their homo- and heterotypic fusion, and finally the egestion of fluid phase from the secretory lysosomes.

Biochemical and Morphological Characterization of Uptake Mechanisms

D. discoideum takes up fluid mainly by macropinocytosis (Hacker *et al.*, 1997), but coated vesicles were found and disruption of clathrin heavy chain leads to an 80% reduction in pinocytosis (O'Halloran and Anderson, 1992; Ruscetti *et al.*, 1994). We tried to further dissect the role of actin, which is crucial for macropinocytic processes (Swanson *et al.*, 1999), and clathrin for fluid phase uptake in *D. discoideum* and to support the findings with our microscopy methods.

We found that 10 μM of the actin-disrupting drug cytochalasin A, which has been shown to inhibit all uptake processes in *D. discoideum* cells assayed in suspension (Hack-

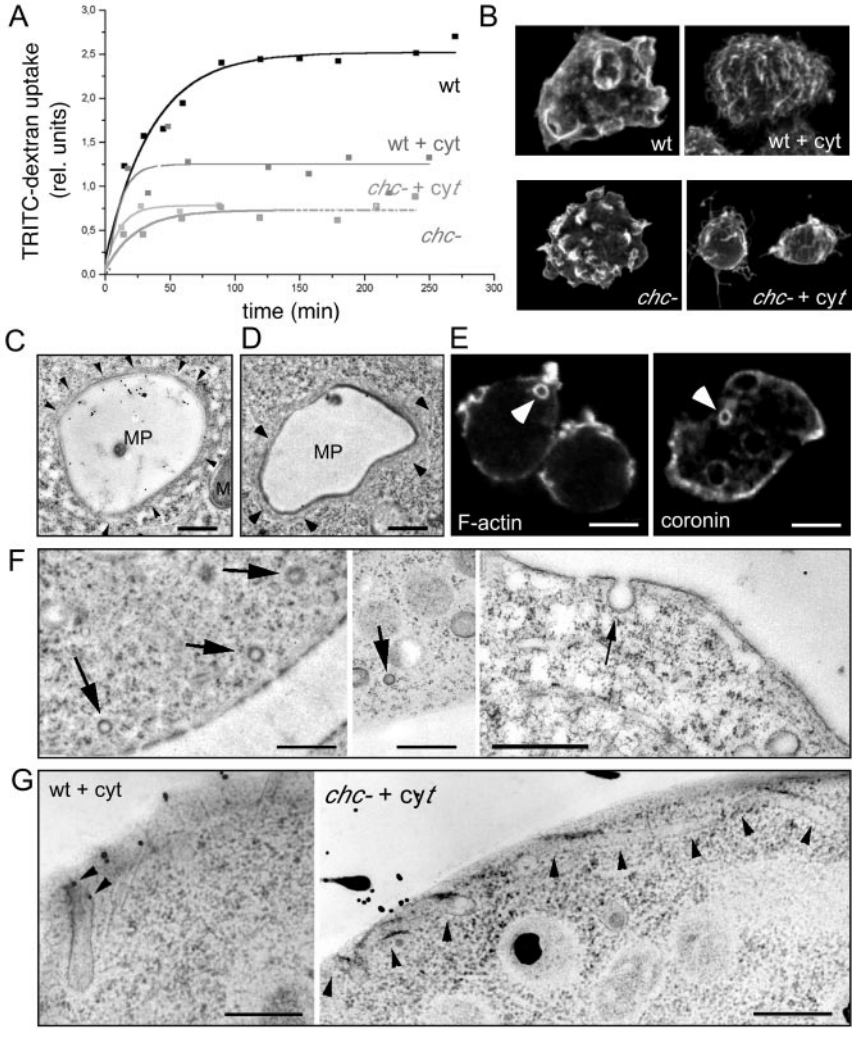

Figure 3. Uptake mechanisms. (A) Uptake of fluorescently labeled dextran as fluid phase marker in wild-type (wt) and *chc*− cells; *chc*− knockout cells showed severe defects in the uptake of fluid phase compared with wild-type cells, as described previously (O'Halloran and Anderson, 1992). Fluid phase endocytosis in wild-type cells was ~50% reduced after disruption of the cytoskeleton with 10 μM cytochalasin A (wt + cyt), whereas fluid phase endocytosis in *chc*− cells (*chc*− + cyt) was not impaired by the same drug treatment. (B) Immunofluorescence staining of the surface of cytochalasin-treated and nontreated wild-type and *chc*− cells. (C and D) Ultrastructure of big endocytic vacuoles (~4 μm in diameter) in wild-type *D. discoideum* cell fed with HRP. These newly formed macropinosomes (MPs) still have an actin cytoskeletal coat, as evidenced by the presence of thin filamentous structures (arrowheads) M, mitochondrium. Bar, 1 μm. (E) Phalloidin staining visualized the actin cortex and intracellular macropinocytic vacuoles (arrowhead) with their F-actin coat (F-actin). Immunofluorescence localization of coronin, an actin-binding protein enriched in the actin cortex, and on macropinocytic vacuoles (arrowhead). Bar, 10 μm. (F) Thin sections of rapidly frozen wild-type cells present small, presumably coated vesicles near the plasma membrane (left) and only noncoated vesicles directly budding from the plasma membrane (right). Bars, 1 μm. (G) EM of cytochalasin A-treated wild-type and *chc*− cells showed extended tubular structures invaginating from the plasma membrane (arrowheads). Bars, 0.5 μm.

er *et al*., 1997), only lead to a 50% reduction in the steady-state level of 70,000-kDa dextran internalized by adherent wild-type cells (Figure 3A, wt). In identical conditions, this concentration of cytochalasin A was sufficient to completely abolish phagocytosis of yeast particles (our unpublished data). Furthermore, in contrast to untreated wild-type cells, we could not identify pinocytic crown- or bowl-shaped structures at the surface of cytochalasin A-treated cells; their surface had a rough appearance with fine filopodia and abundant spikes (Figure 3B, wt and wt + cytA). These observations are a clear indication for actin-independent fluid phase uptake processes. As reported previously (O'Halloran and Anderson, 1992), uptake of the fluid phase marker dextran-TRITC was severely impaired in clathrin heavy chain null (*chc*−) cells (Figure 3A). Surprisingly, the cytochalasin A concentration used to repress macropinocytosis in wild-type cells did not result in a reduction of fluid phase pinocytosis in *chc*− cells (Figure 3A, *chc*− + cytA), although phagocytosis was completely inhibited, controlling for drug sensitivity in these cells under these conditions (our unpublished data). In addition, although cytochalasin treatment caused smoothing of the surface of *chc*− cells (Figure 3B, *chc*− + cyt), even untreated *chc*− cells did not exhibit the well organized cup-like structures seen in wild-type cells, although they show some surface ruffles and spikes (Figure 3B, *chc*−).

A hint for a significant contribution of a micropinocytic uptake mechanism came from the measurement of membrane uptake rate in wild-type cells. We measured uptake rates of plasma membrane proteins by using reversible surface biotinylation and found an internalization rate of one cell surface equivalent every 18 ± 4 min (Neuhaus and Soldati, 2000). We calculated that the observed frequency of five macropinosomes (1.6 μm in diameter) formed per minute (Hacker *et al*., 1997) leads to a membrane uptake rate of 40 μm^2/min. From the upper limit of surface dilation after aspiration of cells with a micropipette, the total cell surface was calculated to be 2.1–2.2-fold the area of the initial spherical shape of the cell in suspension (Evans and Yeung, 1989), and because *D. discoideum* Ax2 cells in suspension have diameters of 12 μm (Schwarz *et al*., 2000) their surface can be calculated to be 973 μm^2. Macropinocytosis thus accounts for the uptake of one cell surface equivalent every 24 min. This value is 33% higher than the observed total membrane uptake rates, and the difference may even be bigger if one takes into account the membrane internalization rates of one cell surface equivalent every 4–10 min reported recently by using another method (Aguado-Velasco and Bretscher, 1999). Macropinocytosis alone is therefore not sufficient to account for the total membrane uptake and micropinocytosis via vesicles with a much bigger surface-to-volume ratio probably operates in parallel, but makes only a minor contribution to the total fluid phase uptake.

To find more precise clues about the dimensions of the structures involved in fluid phase pinocytosis we investigated the uptake of tracer molecules of different sizes in wild-type cells and in clathrin null cells (*chc*− cells) (Ruscetti *et al*., 1994). We used the small 521-kDa dye lucifer yellow and the 2,000,000-kDa TRITC-dextran (Table 1). The size of these molecules was estimated from their structure and from their density and molecular mass to be 1 nm and at least 9 nm, respectively. Fluid phase transit through *D. discoideum* was shown to be linear, and early recycling to the cell surface monitored using 70,000-kDa dextran to be below the level of detection (Aubry *et al*., 1993; Padh *et al*., 1993). Strikingly, even after a relatively short ingestion time the big tracer molecule was preferentially accumulated by wild-type *D. discoideum* cells. Indeed, the fluorescence ratio of TRITC-dextran to lucifer yellow in the medium fed to the cells was 0.21, and after 15 min of incubation the intracellular fluorescence ratio (determined after cell lysis, see MATERIALS AND METHODS) was 0.44. This possibly reflects the balance between uptake and an elusive very early fluid phase recycling. If cells only performed macropinocytosis and engulfed extracellular medium in vacuoles of 1.6-μm average diameter (Hacker *et al*., 1997), no size sorting of marker molecules would be expected. On the other hand, as a function of their "mouth" size, small vesicles (functioning in uptake or recycling) might select small molecules versus large molecules and hence could affect the molecular sorting of their content. Interestingly, in the conditions used *chc*− cells were more dramatically impaired in the uptake of the large marker (10-fold reduction) than of the small marker (20% reduction only), resulting in an intracellular fluorescence ratio of 0.06. Macropinocytosis is therefore probably not the way *chc*− cells manage to ingest medium and survive.

To identify morphologically the uptake structure involved in pinocytosis in *D. discoideum*, we carefully investigated the plasma membrane by EM. In accordance with the finding that *D. discoideum* cells internalize fluid phase mainly by

Table 1. Size selection during the early phase of fluid phase endocytosis

	Dex-TRITC (Fluorescence intensity)	LY (Fluorescence intensity)	Ratio (A. U.)	70 kDa-Dex-TRITC alone (A. U.)
AX2	1.67 ± 0.34 (100%)	3.79 ± 0.66 (100%)	0.44 ± 0.02	100%
AX2 + CytA	0.93 ± 0.14 (56%)	2.74 ± 0.45 (72%)	0.34 ± 0.02	90%
chc−	0.19 ± 0.03 (11%)	3.04 ± 0.67 (80%)	0.06 ± 0.01	37%
chc− + CytA	0.17 ± 0.02 (10%)	1.62 ± 0.23 (43%)	0.11 ± 0.01	50%
Sizes	>9 nm ∅	~1 nm ∅		>3 nm ∅

Effect of absence of clathrin heavy chain and disruption of F-actin. The values shown were taken after 15 min of co-endocytosis of 2,000,000-kDa dextran-TRITC and LY (the fluorescence intensity ratio of TRITC to LY in medium was ~0.21). The values for the uptake of 70-kDa dextran are from the 15-min time point of the curves presented in Figure 5A. As a reference, the fluid phase markers used for EM, HRP, and BSA-Au were ~2.4 nm and ~14 nm in diameter, respectively. A.U., arbitrary units.

forming macropinosomes with a cytoskeletal coat of actin and coronin (Maniak *et al.*, 1995; Hacker *et al.*, 1997), thin filamentous structures were observed on some of the HRP-filled early vacuoles (Figure 3, C and D, arrowheads). Furthermore, fluorescently labeled phalloidin and staining for the F-actin binding protein coronin decorated the periphery of one or a few intracellular vacuoles per cell (Figure 3E, F-actin, coronin). In ~20% of the cells, no staining was visible around intracellular vacuoles, probably because the shedding of the cytoskeletal coat from the vacuole is completed within a minute after internalization (Hacker *et al.*, 1997; Maniak, 1999). We spent great effort to inspect the plasma membrane for small uptake structures. Vesicles of 100-nm diameter with a relatively electron-dense appearance probably resulting from the presence of a (clathrin) coat were observed in the vicinity of the surface (arrows in Figure 3F, left). However, profiles of clathrin-coated vesicles in the process of budding from the plasma membrane were an extreme rarity, almost excluding their contribution to fluid phase and membrane uptake in these cells. It has been postulated that the deficit in budding profiles could also result from an extremely rapid detachment from the plasma membrane and uncoating (Nolta *et al.*, 1994). Alternatively, we sometimes observed small, 100-nm–sized uncoated vesicles in the vicinity of the cell surface or even invaginating from the plasma membrane of wild-type *D. discoideum* cells, offering first morphological hints for the nature of the micropinocytic uptake mechanism in these cells (arrow in Figure 3F, right), but we do not know yet whether the number of these uncoated vesicles will be sufficient to account for the rates of micropinocytosis. To characterize morphologically the endocytic structures involved in the actin- and clathrin-independent pathway, we examined cytochalasin-treated cells by EM. The most striking observation was the presence of fine uncoated tubular structures extending inward from the cell surface in wild-type and in *chc*− cells (Figure 3G). Some of these tubules can be followed for >1 μm from the plasma membrane in a single thin section, indicating a potential underestimation of the total tubule length. Some tubules had gold particles in their lumen, proving that they are involved in fluid phase uptake. In addition, these tubules probably do not belong to the endoplasmic reticulum, because they are not covered with ribosomes and their diameters of 80–100 nm were significantly larger than endoplasmic reticulum tubules (50–60 nm in *D. discoideum*). Some of these tubules seemed to extend along cytoskeletal elements (Figure 3G), which, due to the pharmacological disruption of the F-actin, might be microtubules. In comparison, EM of cytochalasin D-treated HEP-2 cells also revealed an extensive, surface-connected tubular compartment, which was formed by invagination of the plasma membrane in a microtubule-dependent manner and contained transferrin receptors at about the same density as the nontubulated plasma membrane (van Deurs *et al.*, 1996). In that study clathrin-coated pits and caveolae-like structures were infrequently found associated with the tubular membrane. Such a compartment stills functions in fluid phase uptake and may result, in the absence of actin, from the exaggerated microtubule-dependent tubulation of otherwise physiological noncoated endocytic vesicles.

Motility of Endosomal Vesicles

TIRM of living *D. discoideum* cells fed with rhodamine-green dextran revealed the extraordinary dynamics of endosomes. Although some vesicles appeared to constantly move around in a sustained and often bidirectional motion with periodic saltations, others were subjected to oscillations of small amplitude caused by active randomized movement (Lang *et al.*, 2000) (Figure 4A and accompanying Movie 3). For example, a small vesicle was undergoing repeated back-and-forth saltations (Figure 4A, arrow). The short saltatory movements observed are characteristic for movements driven by molecular motors (kinesin and dynein) along

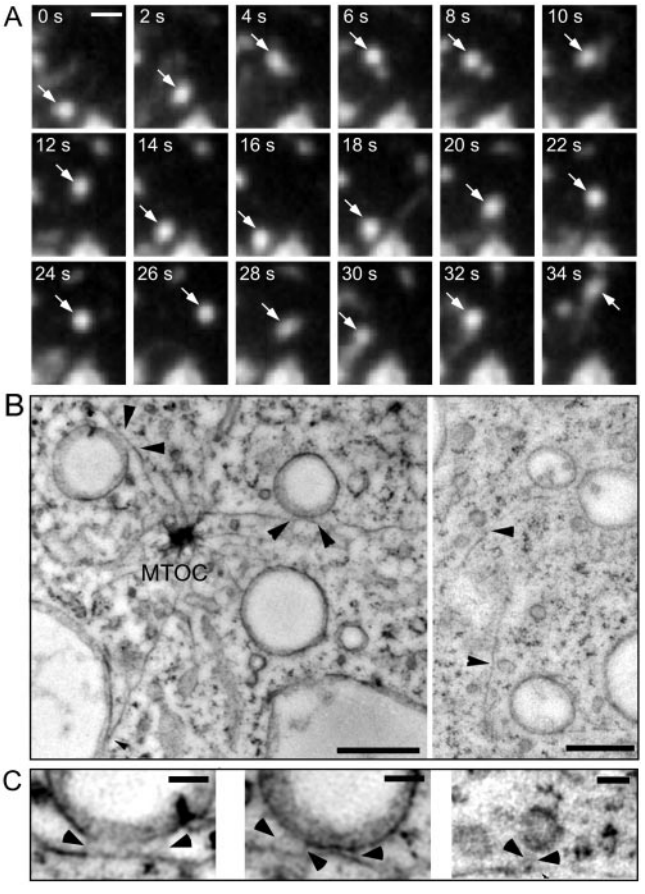

Figure 4. Motility of endocytic vesicles. Wild-type cells were fed with rhodamine-green dextran for 3 h to ensure complete filling of all endocytic compartments and briefly washed with buffer; time-lapse series were recorded with TIRM. (A) A small bright vesicle undergoing rapid saltatory movements is marked by an arrow. The accompanying Movie 3 shows a longer time course (242 s) of the same cell. The movie plays at 6 fps; bars, 2 μm. (B) Ultrastructure of rapidly frozen wild-type *D. discoideum* cells. Vacuoles (470 and 390 nm in diameter) and small vesicles (120–130 nm) bound to microtubules by fine tethers are marked by arrowhead. The distance between microtubules and their bound vacuoles was 13 and 21 nm, respectively. The distance between microtubules and the smaller vesicles was significantly larger (30–40 nm). (C) Higher magnification of the tethers (arrowheads) that connect vacuoles and vesicles to the microtubules. MTOC, Microtubules organizing center. Bars, 0.5 μm (B) and 0.1 μm (C).

microtubules (Allen *et al.*, 1982). This typically bidirectional transport happens in most cells with speeds between 0.5 and 2.0 μm/s (Schroer, 2000). Herein, the speed of the saltatory movement of very small vesicles was measured at 1.9 $\pm$ 0.2 μm/s and slightly slower for larger endosomes, which moved with speeds of 0.7–1.0 μm/s.

Microtubule-based transport of endomembrane structures has already been described in *D. discoideum* cells, which are known to express kinesins and dyneins (Howard *et al.*, 1989; McCaffrey and Vale, 1989; Pollock *et al.*, 1998). Two *D. discoideum* kinesins, *Dd*Unc104, a close relative of *Caenorhabditis elegans* Unc104 and mouse KIF1A, and a 170-kDa protein reconstituted plus end-directed membrane movement in an in vitro assay at 2.62 $\pm$ 0.50 and 1.86 $\pm$ 0.74 μm/s, respectively (Pollock *et al.*, 1999). Furthermore, *Dd*Unc104 was found to be important for organelle transport in vivo, because its absence dramatically reduced overall organelle movements (Pollock *et al.*, 1999). The velocities for saltatory movements of endocytic vesicles we observed in vivo correspond well to the reported in vitro data, an indication that endosomes may be transported by such kinesins along microtubules.

Endosomal vacuoles were connected to microtubules extending from the microtubule organizing center via thin tethers (Figure 4, B and C), possibly representing motor proteins (Hirokawa *et al.*, 1989). EM investigations have revealed that latex beads covered with bovine brain kinesin were bound to microtubules via 25–30-nm-long structures (Bloom *et al.*, 1989). Interestingly, there appears to be a correlation between the size of the vacuoles, the length of the tether, and the speed of movement. Vacuoles between 0.5 and 1.5 μm in diameter were bound to microtubules (Figure 4B, higher magnification can be seen in Figure 4C) within an average distance of 18 nm. Vacuoles of this size moved with speeds of 0.7–1.0 μm/s, whereas faster saltatory movements of 2 μm/s were observed for smaller vesicles. By EM, such small vesicles of ~120 nm in diameter were connected to the microtubules by 35–40-nm-long tethers (Figure 4B, higher magnification can be seen in the rightmost panel of Figure 4C). Overall, our findings are consistent with earlier observations of bidirectional movement of organelles in *D. discoideum* (Roos *et al.*, 1987; Pollock *et al.*, 1999).

Endosome Tubulation and Multivesicular Bodies

Tubular structures can be observed in living *D. discoideum* cells by TIRM to extend from morphologically different types of endosomes (Figure 5A, arrowheads and accompanying Movie 4; also higher magnification in Figure 5C, arrowheads). Some of the intensely labeled late endosomal vacuoles were not filled homogeneously with the internalized marker molecules (Figure 5A, asterisk, and higher magnification in Figure 5B, arrows), an indication that they contained internal membranes that exclude the dye. In addition, the vacuole (3–5 μm in diameter) appeared to rotate around its axis and repeatedly extended tubular structures (Figure 5B, arrowheads), some up to 5 μm in length. These tubular structures extended rapidly at several micrometers per second, similar to the speeds observed for the transport of small endocytic vesicles (Figure 4). In animal cells, tubular structures extend from endosomes and lysosomes along microtubules (Matteoni and Kreis, 1987), driven by kinesins (Hollenbeck and Swanson, 1990). In addition, tubular structures extending from the Golgi apparatus toward the surface of animal cells move with the help of kinesins at ~0.5 μm/s (Kreitzer *et al.*, 2000).

In perfect correlation with this observation in live *D. discoideum* cells and as in early endosomes (Figure 2), tubular structures that extend from late endosomes containing aggregated gold particles can also be documented by EM (Figure 5E, arrowheads, and arrows in 5D). In addition, after longer internalization times (30 min) some endosomal vacuoles filled with aggregated gold particles contained internal membranous structures (Figure 5D, arrowheads), probably corresponding to the endocytic structures observed by TIRM (Figure 5A). Mammalian cells also contain spherical compartments of 0.5–1.5-μm diameter with internal membranes that were originally termed multivesicular compartment or bodies (Griffiths *et al.*, 1989; Gruenberg *et al.*, 1989; McDowall *et al.*, 1989; Killisch *et al.*, 1992). These compartments bud from the early endosomes and serve as endosomal carrier vesicles for the transport of material to the late endosomes (Gu and Gruenberg, 1999). Multivesicular compartments with low electron densities were also described in yeast (Hicke *et al.*, 1997; Prescianotto-Baschong and Riezman, 1998).

Small Vesicles Cluster around Bigger Endosomal Vacuoles

Another example of a typical *D. discoideum* endocytic profile is shown in Figure 6. TIRM revealed that some bright endosomal vacuoles seemed to be tethered to smaller vesicles because a vacuole with associated vesicles appeared to move through the cell as a unit for prolonged periods of time (Figure 6A and accompanying Movie 5). Such chains of small vesicles, which continuously changed their relative position, but nevertheless seemed tethered to each other and/or to frequently contact the central vacuole (Figure 6A, star), were observed for up to 5 min.

Large vacuoles surrounded by numerous vesicular profiles (200–300 nm in diameter), perfectly corroborating the live observations were seen by EM. The extreme example of Figure 6D presents a vacuole without gold particles but, due to the relatively electron-dense lumen and the proximity of other filled vacuoles, it can be assumed to belong to the endo-lysosomal system. In addition, in agreement with the frequent accumulation of small vesicles around big endosomal vacuoles observed by EM and in living cells, immunofluorescence localization revealed that a major fraction of the lysosomal enzymes was found in "rings of dots" (Figure 6B), punctate structures clustered around large vacuoles (see also higher magnifications in Figure 6B); some staining may also be inside the endosomal vacuoles in the form of small peripheral clumps (Figure 6B). This accumulation of vesicles with high concentrations of lysosomal enzymes could reflect the process of delivery of hydrolases into the endosomal vacuoles and/or their retrieval at the end of the endocytic pathway, before final egestion.

Endosome-Endosome Fusion

Endosomal vacuoles in *D. discoideum* frequently contacted each other (Movies 1 and 5), a potential sign of partial "kiss-and-run" fusion (Desjardins *et al.*, 1994), and complete fusion events were only occasionally observed. An example

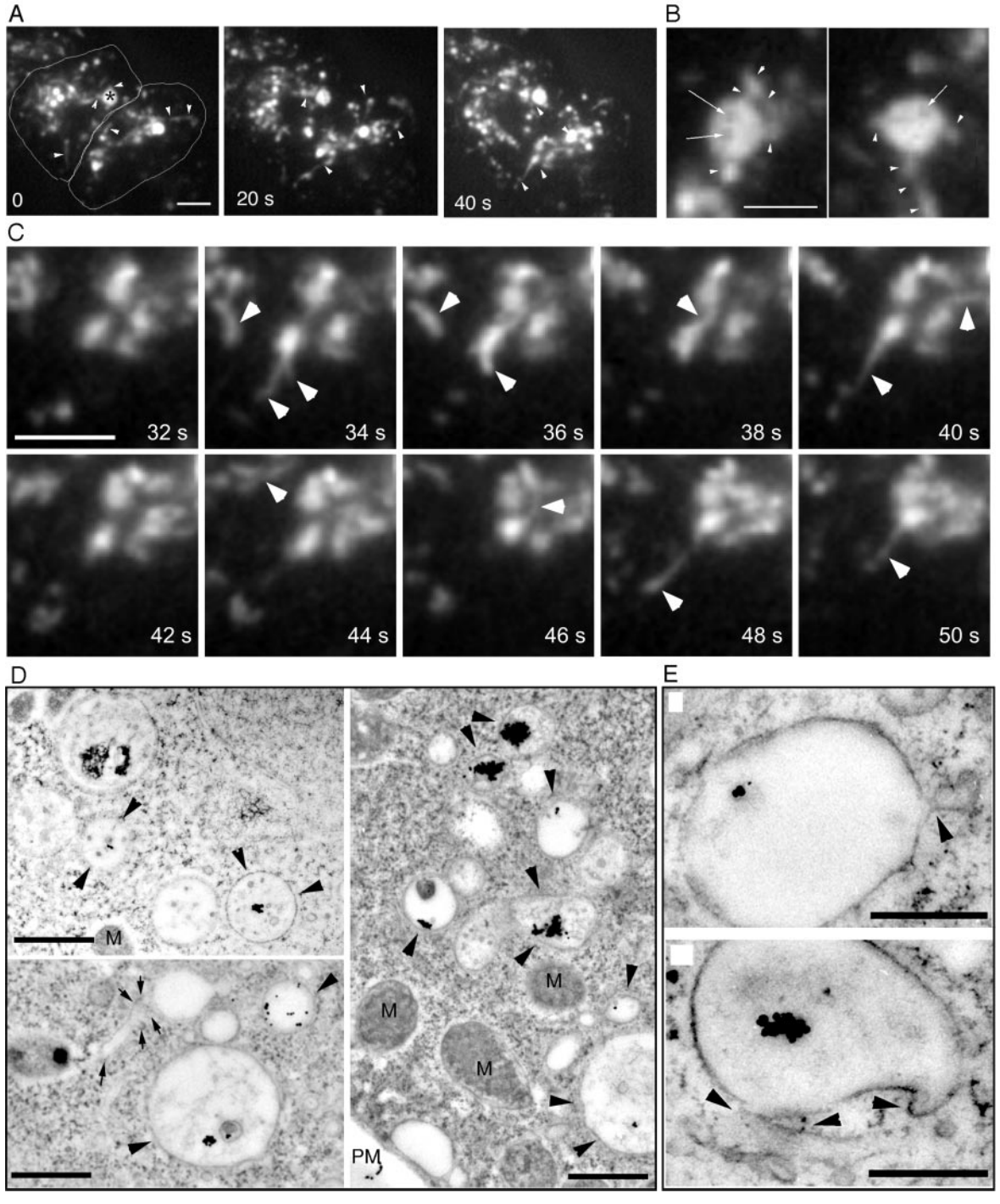

Figure 5. Tubules and multivesicular bodies. (A) Wild-type cells were fed with rhodamine-green dextran for 30 min and briefly washed with buffer; time-lapse series were recorded with TIRM. The cell boundaries are outlined in the first frame. A very dynamic vacuole with intermediate dextran concentration in the upper left cell (asterisk) repeatedly extended tubular structures (arrowheads); other tubular structures are also marked by arrowheads. The accompanying Movie 4 shows a longer time course (242 s) of the same cell. The movie plays at 6 fps; bar, 10 μm. (B) Selected frames of the vacuole marked by an asterisk in A at a higher magnification, showing again the repeated extension of tubular structures (arrowheads). In addition, the vacuole was inhomogeneously filled with dextran, dark patches in the vacuolar lumen are marked by arrows. Bar, 5 μm. (C) Higher magnification of a vacuole that repeatedly extended tubular structures (arrowheads). Bar, 2 μm. (D) Ultrastructure of endosomes in wild-type *D. discoideum* cells that ingested BSA-Au particles for 30 min. Some endosomal vacuoles contained internal membranes and aggregated gold particles (arrowheads), a tubular structure is marked by arrows. Bars, 1 μm. (E) Higher magnification of late endosomal vacuoles with extending tubular structures (arrowheads). M, mitochondria. Bars, 0.5 μm.

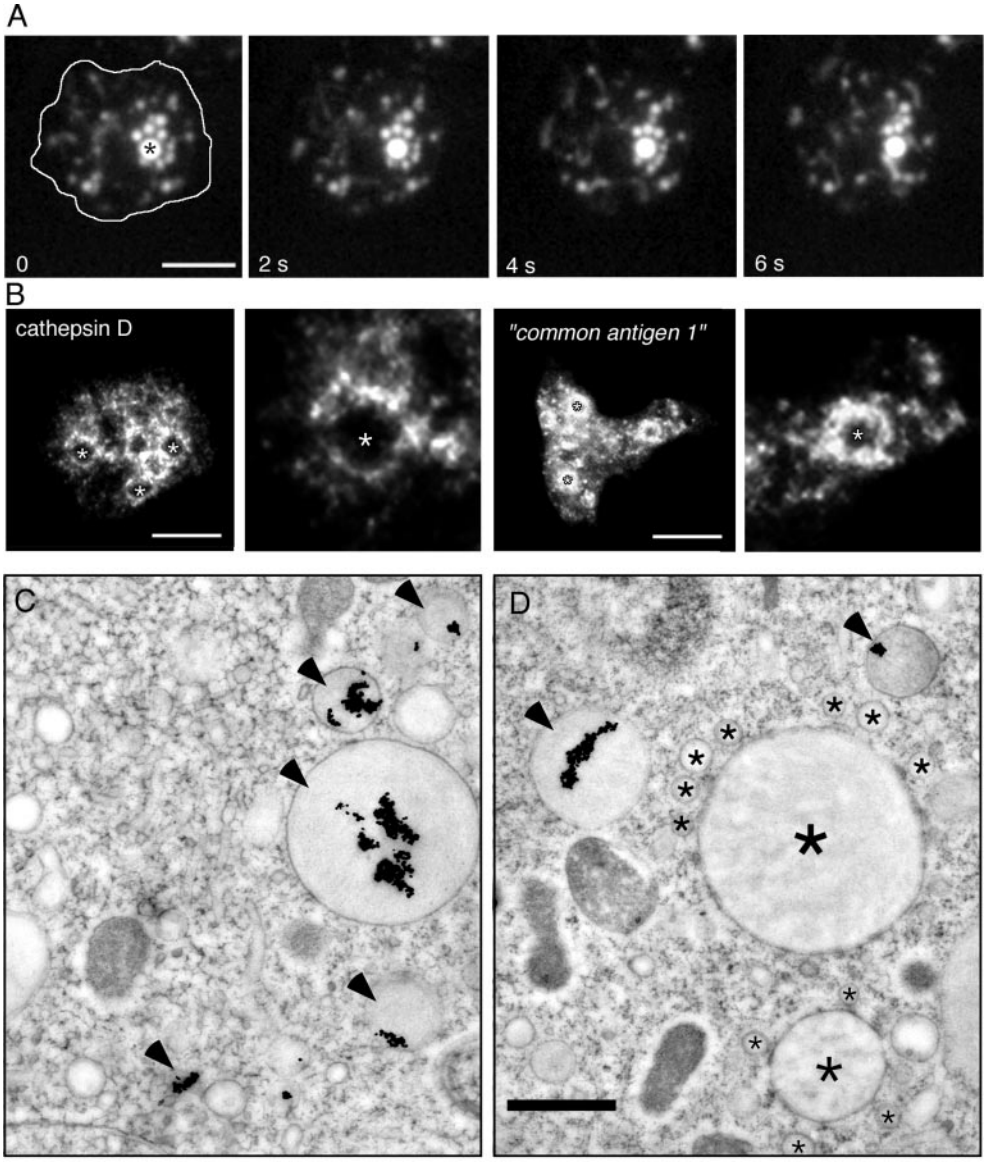

Figure 6. Clusters. (A) Wild-type cells were fed with rhodamine-green dextran for 60 min and briefly washed with buffer; time-lapse series were recorded with TIRM. The cell boundaries are outlined in the first frame. The big central vacuole (asterisk) was surrounded by smaller vesicular structures that continuously moved around and repeatedly contacted this vacuole. The accompanying Movie 5 shows a longer time course (242 s) of the same cell. The movie plays at 6 fps; bar, 10 μm. (B) Immunofluorescence localization of lysosomal enzymes. Antibodies against cathepsin D and against the "common antigen 1," a mannose-6-sulfate–containing carbohydrate epitope present on *D. discoideum* lysosomal enzymes such as α-mannosidase and β-glucosidase (Knecht *et al.*, 1984; Freeze *et al.*, 1990), labeled small vesicular structures, that formed "rings of dots" around bigger, unlabeled vacuoles (marked by asterisks and also shown in higher magnification). Bar, 10 μm. (C and D) Ultrastructure of late endosomes in wild-type *D. discoideum* cells that ingested BSA-Au particles for 60 min. Late endosomes were characterized by electron dense lumen and strongly aggregated gold particles (arrowheads). Some endosomal vacuoles with dark lumen (big asterisk) were surrounded by smaller vesicular structures (small asterisks) reminiscent of the situation in A. Bar, 1 μm.

of a complete fusion event between two vacuoles, which first moved for ~4 min connected to each other through the cell, is shown in Figure 7A, and the accompanying Movie 6. The situation in mammalian cells is similar; complete fusion between endosomes is only a rare event, which has been explained by the slow dissociation of the fusion complex (Roberts *et al.*, 1999). In addition, stable preexisting compartments (according to the model from Griffiths and Gruenberg (1991) and Griffiths (1996) that acquire endocytosed fluid phase marker molecules via fusion with small transient transport vesicles appeared to exist in *D. discoideum*. Figure 7B and the accompanying Movie 7 show a large vacuole, which did not visibly contain endocytic marker at the beginning of the recording (arrowheads), but was visible as a ring due to association with small dextran-filled vesicles. It was gradually filled to a significant concentration in a 3-min period by fusion with small, dextran-filled vesicles (Figure 7C, arrowheads).

This process requires the close apposition of these compartments, a docking reaction, and membrane fusion. Numerous studies using time-lapse microscopy techniques have documented fusion among endocytic vesicles in a variety of cell types, including macrophages (Lewis, 1931) and fibroblasts (Willingham and Yamada, 1978). Short contacts between newly built pinosomes and lysosome-like structures in fibroblasts caused the destruction of the pinosomes by "piranhalysis" (Willingham and Yamada, 1978). However, morphological descriptions of the membrane merger process occurring during endosome fusion are extremely rare. Study of cryo-immobilized and freeze-substituted *D. discoideum* cells at the EM level revealed that the membranes of some vacuoles were in tight contact and fusion events

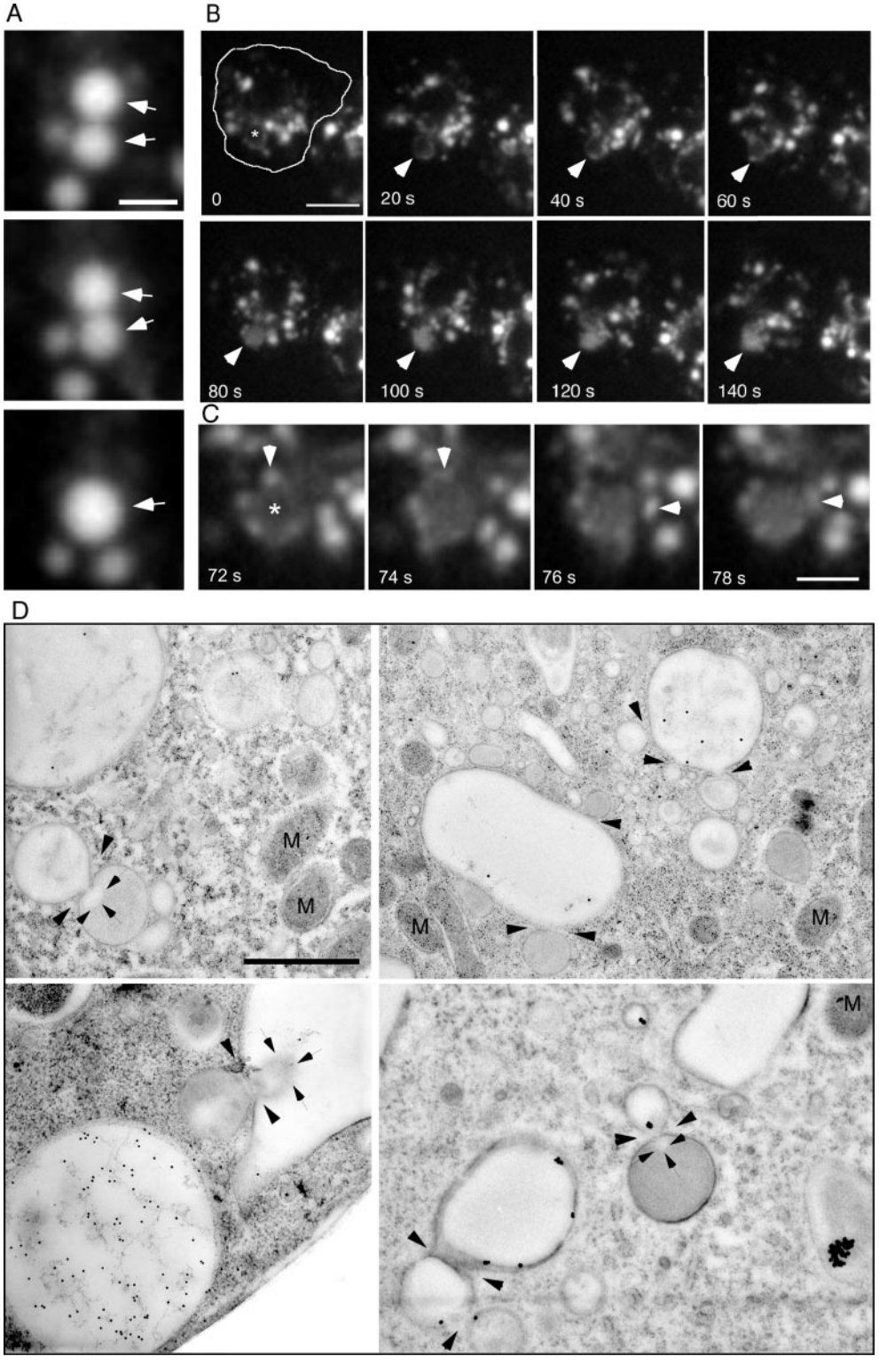

Figure 7. Endosome-endosome fusion. Wild-type cells were fed with rhodamine-green dextran for 30 min and briefly washed with buffer; time-lapse series were recorded with TIRM. The cell boundaries are outlined in the first frame. (A) Two bigger vacuoles that moved together through the cell for some minutes finally fused with each other (arrowheads). The accompanying Movie 6 shows a longer time course (252 s) of the same cell. (B) A big vacuole (asterisk and then arrowhead), that was barely visible in the first frames, repeatedly fused with small vesicles, and thereby was slowly filled with fluid phase marker in roughly 4 min. (C) Higher magnification of the vacuole marked in B, small vesicles fusing with this vacuole are marked by arrowheads. The accompanying Movie 7 shows a longer time course (242 s) of the same cell. The movies play at 6 fps; bars, 2 μm (A), 5 μm (C), and 10 μm (B). (C) Ultrastructure of fusion events between endocytic vacuoles in wild-type *D. discoideum* cells (arrowheads). Note the plumes of differentially electron-dense lumenal material (arrows) diffusing through some of the fusion pores. M, mitochondria. Bar, 1 μm.

between morphologically similar or different endosomal vacuoles were captured. Remarkably, there seemed to be exchange of differentially electron-dense lumenal material, visualized as jets or plumes (Figure 7D, delimited by arrows) projecting from the site of fusion (arrowheads). In mammalian cells early and late endosomes undergo homotypic but

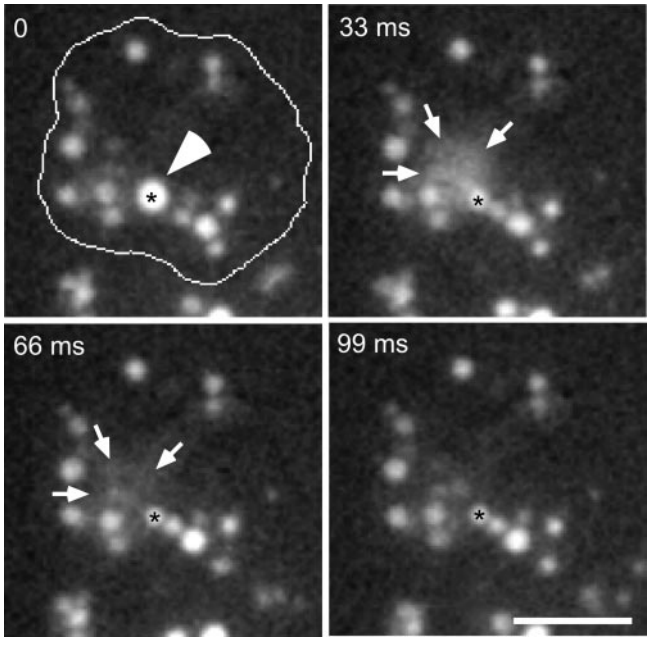

Figure 8. Exocytosis from the secretory lysosomal compartment. Wild-type cells were fed with rhodamine-green dextran for 2 h and briefly washed with buffer; time-lapse series were recorded with TIRM. The cell boundaries are outlined in the first frame. A big, bright vacuole (asterisk and arrowhead) was almost immobile for some minutes. It suddenly fused with the plasma membrane and egested its content in the extracellular space in the form of a cloud of staining (delimited by arrows). Note that fusion was not complete, because a remnant of the secretory lysosome was still visible after egestion. The accompanying Movie 8 shows a longer time course (1.7 s) of the same cell, it plays at 6 fps; bar, 10 μm.

not heterotypic fusion events (Gruenberg and Clague, 1992; Griffiths, 1996). Herein, the fusion pores between the endosomal vacuoles had diameters of 50–150 nm, perhaps depending on the stage of the fusion event. It was shown recently, that during fusion events in GFP-Rab5 overexpressing mammalian cells, the endosomes are often connected to each other via very thin cytoplasmic bridges, through which membrane material is exchanged (Roberts *et al.*, 1999). The fact that narrow fusion pores are observed relatively frequently in *D. discoideum* fits well with our TIRM data (Figure 7, A–C).

Exocytosis from Secretory Lysosomes

At the end of the endosomal pathway *D. dictyostelium* egests excess fluid and undigested remnants from a nearly neutral compartment (Aubry *et al.*, 1993; Jenne *et al.*, 1998). These secretory lysosomes are surrounded by a coat consisting of F-actin and vacuolin (Rauchenberger *et al.*, 1997; Jenne *et al.*, 1998), which was also found in patches below the plasma membrane (Jenne *et al.*, 1998), indicating that it is involved in exocytosis from this compartment. By using TIRM and video equipment, dynamic processes were recorded with rates of 30 frames/s. We were able to document that egestion indeed happens via direct exocytosis from the secretory lysosomes (Figure 8 and accompanying Movie 8). A micrometer-sized intensely labeled vacuole (diameter 2.4 $\pm$ 0.2 μm, black asterisk) was first immobile for some minutes, probably docked at the plasma membrane. It suddenly released its content into the extracellular medium, where the dextran molecules rapidly diffused away, resulting in a cloud of fluorescence (delimited by arrows) that disappeared in ~60 ms. Because the vacuole was still visible after the exocytic event (black asterisk), it seems to have egested only part of its content. The extreme transience of exocytosis may explain why this process has not been observed by confocal microscopy.

Endocrine cells release peptide hormones from large, dense-core secretory granules, which move actively to the plasma membrane and are reversibly anchored at their docking sites before exocytosis (Steyer *et al.*, 1997). Exocytosis in these cells is coupled tightly to endocytic events at high concentrations of extracellular calcium ions, such that secretory vesicles fuse transiently with the plasma membrane before being internalized (the kiss-and-run mechanism) (Ales *et al.*, 1999). On the other hand, endocytosis occurs by an independent process after complete incorporation of secretory vesicle into the plasma membrane at low calcium concentrations (Ales *et al.*, 1999) and it was proposed that, during secretion of neurotransmitters at synapses, the mode of exocytosis is modulated by calcium to attain optimal conditions for coupled exocytosis and endocytosis according to synaptic activity (Ales *et al.*, 1999). Exocytosis from the secretory lysosomes and endocytosis (macropinocytosis) in *D. discoideum* are not directly linked like exo- and endocytosis in endocrine cells. Macropinosomes are newly formed from actin-containing cell surface extensions. Whether both processes are temporally or spatially linked is an interesting topic for future investigations. From the size of the exocytic compartments, secretory lysosomes in *D. discoideum* are more similar to the granules in horse eosinophils, which undergo compound exocytosis. Granule-granule fusion occurs inside the cell, forming large compound granules that then fuse with the plasma membrane and release all their content through one fusion pore (Scepek and Lindau, 1993).

CONCLUSION

The original description of the endocytic pathway, the membrane and solute transport from the plasma membrane to the degradative compartment mainly relied on broad morphological studies of animal cells. The introduction of genetic approaches to study endocytosis accelerated the identification of molecules required for this process, and the isolation of endocytosis mutants in budding yeast has been especially successful in this respect. However, the intrinsic difficulties with ultrastructural studies in yeast make comparisons to animal cells difficult. *D. discoideum* cells have high rates of endocytosis and are, like animal cells, dependent on endocytosis for nutrition. Most importantly, their overall morphology is very reminiscent of leukocytes and genetics in this organism is straightforward. *D. discoideum* therefore offers unique advantages as a model system for the investigation of endocytic processes because it allows the combination of genetic, biochemical, and morphological studies.

These fundamentally invaluable characteristics were somewhat compensated for by the technical difficulties to

surmount the extreme dynamics of its endomembrane system and its high sensitivity toward osmotic changes and light. Therefore, up to now, relatively little was known about the morphology of the endocytic compartments and the distinct membrane-trafficking steps involved. The correlation of evanescent wave microscopy with electron microscopy of rapidly frozen samples allowed us to visualize and confirm the existence of distinct organelles along the endocytic pathway, including primary endocytic vesicles of very different sizes and vesicular-tubular structures that may be the *D. discoideum* analogs of early and late endosomes and lysosomes. These technical advances revealed much stronger connections and similarities to animal cells than originally thought. For example, contrary to yeast, *D. discoideum* appears to operate at least three different endocytic routes, including macro- and micropinocytosis and phagocytosis. In addition, even although caveolae are absent, rafts have been identified and appear to play a role in signaling (Xiao and Devreotes, 1997) and cell-cell adhesion (Harris *et al.*, 2001). Their involvement in endocytosis has not yet been investigated. Our evidence allowed to biochemically and morphologically distinguish actin-dependent and actin-independent uptake mechanisms. Macropinocytosis appears to account for most of the fluid phase uptake but it is supplemented by a (clathrin-independent) micropinocytic process, which accounts for about half of the membrane uptake but only for a minor part of fluid phase endocytosis. Similar results were found in cells belonging to the immune system, which are morphologically very similar to *D. discoideum*; fluid phase endocytosis via clathrin-coated vesicles makes up only 16% of total fluid phase uptake in leukocytes and negligible amounts in macrophages (Daukas and Zigmond, 1985). Because *D. discoideum* cells are dependent on endocytosis for nutrient uptake, the presence of several mechanisms may be essential for survival. In addition, the existence of multiple uptake pathways probably allows for transport of ingested material to different intracellular compartments, for higher flexibility, adaptability to environmental conditions, and differential regulation. For example, in animal cells, clathrin-independent endocytosis at the apical surface of polarized epithelial cells is selectively regulated by cAMP (Eker *et al.*, 1994) and uptake via caveolae can selectively be regulated by phosphorylation (Smart *et al.*, 1993; Parton *et al.*, 1994).

We showed that early endosomes have a tubular/vesicular morphology and are distributed throughout the cytoplasm, similar to that in mammalian cells (Wall *et al.*, 1980; Geuze *et al.*, 1983; Hopkins and Trowbridge, 1983). Comparably to late endosomes and lysosomes in animal cells, after longer internalization times in *D. discoideum*, a diversity of vesicular and tubular structures as well as multivesicular compartments appear. These endo-lysosomal organelles move with speeds of several micrometers per second and are probably powered along microtubules by kinesins and/or dynein. Late endosomes and secretory lysosomes seem to cluster together, to have frequent contacts, and to undergo repeated homotypic and heterotypic fusion events.

Altogether, *D. discoideum* appears as a powerful organism to perform a combination of biochemical, genetic, and cell biological studies of endocytosis and phagocytosis/macropinocytosis, processes that either do not function in some model organisms or are very difficult to approach. The present investigation defines the blueprints for such further detailed analyses.

ACKNOWLEDGMENTS

We thank Drs. M.I. Geli (University of Heidelberg, Germany) and M. Maniak (Universität GhK, Kassel, Germany) for helpful comments on the manuscript. We also thank Drs. Jürgen Steyer (University of California, Berkeley, CA) and T. Lang (MPI for Biophysical Chemistry, Göttingen, Germany) for help with the evanescent wave microscopy, and Heinz Horstmann (MPI for Medical Research, Heidelberg, Germany) for help with electron microscopy. Drs. J. Garin (CEA, Grenoble, France) and M. Maniak and G. Gerisch (MPI for Biochemistry, Martinsried, Germany) kindly provided antibodies. A special thanks goes to Dr. T. O'Halloran (University of Texas, Austin, TX) for the gift of *chc*− cells. The work was supported by the Max-Planck Society and a grant from the Deutsche Forschungsgemeinschaft to T.S. (SFB 352). E.M.N. was successively a recipient of doctoral and postdoctoral fellowships from the Max-Planck Society.

REFERENCES

Aguado-Velasco, C., and Bretscher, M. (1999). Circulation of plasma membrane in *Dictyostelium*. Mol. Biol. Cell. *10*, 4419–4427.

Ales, E., Tabares, L., Poyato, J.M., Valero, V., Lindau, M., and Alvarez de Toledo, G. (1999). High calcium concentrations shift the mode of exocytosis to the kiss-and-run mechanism. Nat. Cell Biol. *1*, 40–44.

Allen, R., Metuzals, D., Tasaki, I., Brady, S., and Gilbert, S. (1982). Fast axonal transport in squid giant axon. Science *218*, 1127–1129.

Aubry, L., Klein, G., Martiel, J.L., and Satre, M. (1993). Kinetics of endosomal pH evolution in *Dictyostelium discoideum* amoebae - study by fluorescence spectroscopy. J. Cell Sci. *105*, 861–866.

Aubry, L., Klein, G., Martiel, J.L., and Satre, M. (1997). Fluid-phase endocytosis in the amoebae of the cellular slime mold *Dictyostelium discoideum*: mathematical modeling of kinetics and pH evolution. J. Theor. Biol. *184*, 89–98.

Baker, J.R. (1968). Principles of Biological Microtechnique: A Study of Fixation and Dyeing, New York: John Wiley & Sons.

Bereiter-Hahn, J., and Voeth, M. (1979). Metabolic state dependent preservation of cells by fixatives for electron microscopy. Microsc. Acta *82*, 239–250.

Bloom, G.S., Wagner, M.C., Pfister, K.K., and Brady, S.T. (1989). Native structure and physical properties of bovine brain kinesin and identification of the ATP-binding subunit polypeptide. Cell *56*, 867–878.

Bright, N.A., Reaves, B.J., Mullock, B.M., and Luzio, J.P. (1997). Dense core lysosomes can fuse with late endosomes and are reformed from the resultant hybrid organelles. J. Cell Sci. *110*, 2027–2040.

Daukas, G., and Zigmond, S.H. (1985). Inhibition of receptor-mediated, but not fluid-phase endocytosis in polymorphonuclear leukocytes. J. Cell Biol. *101*, 1673–1679.

de Chastellier, C., and Ryter, A. (1977). Changes of the cell surface and of the digestive apparatus of *Dictyostelium discoideum* during the starvation period triggering aggregation. J. Cell Biol. *75*, 218–36.

de Chastellier, C., Ryter, A., and Thilo, L. (1983). Membrane shuttle between plasma membrane, phagosomes, and pinosomes in *Dictyostelium discoideum* amoeboid cells. Eur. J. Cell Biol. *30*, 233–243.

de Hostos, E.L., Rehfuess, C., Bradtke, B., Waddell, D.R., Albrecht, R., Murphy, J., and Gerisch, G. (1993). *Dictyostelium* mutants lacking

the cytoskeletal protein coronin are defective in cytokinesis and cell motility. J. Cell Biol. *120*, 163–173.

Denzer, K., Kleijmeer, M.J., Heijnen, H.F., Stoorvogel, W., and Geuze, H.J. (2000). Exosome: from internal vesicle of the multivesicular body to intercellular signaling device. J. Cell Sci. *113*, 3365–3374.

Desjardins, M., Huber, L.A., Parton, R.G., and Griffiths, G. (1994). Biogenesis of phagolysosomes proceeds through a sequential series of interactions with the endocytic apparatus. J. Cell Biol. *124*, 677–688.

Eker, P., Holm, P.K., van Deurs, B., and Sandvig, K. (1994). Selective regulation of apical endocytosis in polarized Madin-Darby canine kidney cells by mastoparan and cAMP. J. Biol. Chem. *269*, 18607–18615.

Evans, E., and Yeung, A. (1989). Apparent viscosity and cortical tension of blood granulocytes determined by micropipet aspiration. Biophys. J. *56*, 151–160.

Favard-Sereno, C., Ludosky, M.A., and Ryter, A. (1981). Freeze-fracture study of phagocytosis in *Dictyostelium discoideum*. J. Cell Sci. *51*, 63–84.

Fok, A.K., Clarke, M., Ma, L., and Allen, R.D. (1993). Vacuolar H-ATPase of *Dictyostelium discoideum*: a monoclonal antibody study. J. Cell Sci. *106*, 1103–1113.

Freeze, H.H., Bush, J.M., and Cardelli, J. (1990). Biochemical and genetic analysis of an antigenic determinant found on N-linked oligosaccharides in *Dictyostelium*. Dev. Genet. *11*, 463–472.

Fukui, Y., Yumura, S., and Yumura, T.K. (1987). Agar-overlay immunofluorescence: high-resolution studies of cytoskeletal components and their changes during chemotaxis. In: Methods Cell Biology, vol 28, ed. J.A. Spudich, Orlando, FL: Academic Press, 347–356.

Geli, M.I., and Riezman, H. (1998). Endocytic internalization in yeast and animal cells: similar and different. J. Cell Sci. *111*, 1031–1037.

Geuze, H.J., Slot, J.W., Strous, G.J., Lodish, H.F., and Schwartz, A.L. (1983). Intracellular site of asialoglycoprotein receptor-ligand uncoupling: double-label immunoelectron microscopy during receptor-mediated endocytosis. Cell *32*, 277–287.

Griffiths, G. (1993). Fine Structure Immunocytochemistry, Berlin: Springer.

Griffiths, G. (1996). Secretory lysosomes - a special mechanism of regulated secretion in hemopoietic cells. Trends Cell Biol. *6*, 329–332.

Griffiths, G., Back, R., and Marsh, M. (1989). A quantitative analysis of the endocytic pathway in baby hamster kidney cells. J. Cell Biol. *109*, 2703–2720.

Griffiths, G., and Gruenberg, J. (1991). The arguments for pre-existing early and late endosomes. Trends Cell Biol. *1*, 5–9.

Griffiths, G., McDowall, A.W., Back, R., and Dubochet, J. (1984). On the preparation of cryosections for immunocytochemistry. J. Ultrastruct. Res. *89*, 65–78.

Gruenberg, J., and Clague, M.J. (1992). Regulation of intracellular membrane transport. Curr. Opin. Cell Biol. *4*, 593–599.

Gruenberg, J., Griffiths, G., and Howell, K.E. (1989). Characterization of the early endosome and putative endocytic carrier vesicles in vivo and with an assay of vesicle fusion in vitro. J. Cell Biol. *108*, 1301–1316.

Gruenberg, J., and Howell, K. (1987). An internalized transmembrane protein resides in a fusion-competent endosome for less than 5 minutes. Proc. Natl. Acad. Sci. USA *84*, 5758–5762.

Gu, F., and Gruenberg, J. (1999). Biogenesis of transport intermediates in the endocytic pathway. FEBS Lett. *452*, 61–66.

Hacker, U., Albrecht, R., and Maniak, M. (1997). Fluid-phase uptake by macropinocytosis in *Dictyostelium*. J. Cell Sci. *110*, 105–112.

Harris, T.J., Awrey, D.E., Cox, B.J., Ravandi, A., Tsang, A., and Siu, C.H. (2001). Involvement of a triton-insoluble floating fraction in *Dictyostelium* cell-cell adhesion. J. Biol. Chem. *276*, 18640–18648.

Hasty, D.L., and Hay, A.R. (1978). Freeze-fracture studies of the developing cell surface. II. Particle-free membrane blisters on glutaraldehyde-fixed corneal fibroblasts are artifacts. J. Cell Biol. *78*, 756–768.

Hed, J. (1986). Methods for distinguishing ingested from adhering particles. Methods Enzymol. *132*, 198–204.

Hicke, L., Zanolari, B., Pypaert, M., Rohrer, J., and Riezman, H. (1997). Transport through the yeast endocytic pathway occurs through morphologically distinct compartments and requires an active secretory pathway and Sec18p/N-ethylmaleimide-sensitive fusion protein. Mol. Biol. Cell *8*, 13–31.

Hirokawa, N., Pfister, K.K., Yorifuji, H., Wagner, M.C., Brady, S.T., and Bloom, G.S. (1989). Submolecular domains of bovine brain kinesin identified by electron microscopy and monoclonal antibody decoration. J. Cell Biol. *108*, 1453–1463.

Hollenbeck, P.J., and Swanson, J.A. (1990). Radial extension of macrophage tubular lysosomes supported by kinesin. Nature *346*, 864–866.

Hopkins, C.R., Gibson, A., Shipman, M., and Miller, K. (1990). Movement of internalized ligand-receptor complexes along a continuous endosomal reticulum. Nature *346*, 335–339.

Hopkins, C.R., and Trowbridge, I.S. (1983). Internalization and processing of transferrin and the transferrin receptor in human carcinoma A431 cells. J. Cell Biol. *97*, 508–521.

Howard, J., Hudspeth, A.J., and Vale, R.D. (1989). Movement of microtubules by single kinesin molecules. EMBO J. *8*, 3229–3234.

Humbel, B.M., and Biegelmann, E. (1992). A preparation protocol for postembedding immunoelectron microscopy of *Dictystelium discoideum* cells with monoclonal antibodies. Scanning Microsc. *6*, 817–825.

Jenne, N., Rauchenberger, R., Hacker, U., Kast, T., and Maniak, M. (1998). Targeted gene disruption reveals a role for vacuolin B in the late endocytic pathway and exocytosis. J. Cell Sci. *111*, 61–70.

Journet, A., Chapel, A., Jehan, S., Adessi, C., Freeze, H., Klein, G., and Garin, J. (1999). Characterization of *Dictyostelium discoideum* cathepsin D. Molecular cloning, gene disruption, endo-lysosomal localization and sugar modifications. J. Cell Sci. *112*, 3833–3843.

Killisch, I., Steinlein, P., Romisch, K., Hollinshead, R., Beug, H., and Griffiths, G. (1992). Characterization of early and late endocytic compartments of the transferrin cycle. Transferrin receptor antibody blocks erythroid differentiation by trapping the receptor in the early endosome. J. Cell Sci. *103*, 211–232.

Knecht, D.A., Dimond, R.L., Wheeler, S., and Loomis, W.F. (1984). Antigenic determinants shared by lysosomal proteins of *Dictyostelium discoideum*. Characterization using monoclonal antibodies and isolation of mutants affecting the determinant. J. Biol. Chem. *259*, 10633–10640.

Kreitzer, G., Marmorstein, A., Okamoto, P., Vallee, R., and Rodriguez-Boulan, E. (2000). Kinesin and dynamin are required for post-Golgi transport of a plasma-membrane protein. Nat. Cell Biol. *2*, 125–127.

Lang, T., Wacker, I., Wunderlich, I., Rohrbach, A., Giese, G., Soldati, T., and Almers, W. (2000). Role of actin cortex in the subplasmalemmal transport of secretory granules in PC-12 cells. Biophys. J. *78*, 2863–2877.

Lewis, W.H. (1931). Pinocytosis. Bull. Johns Hopkins Hosp. *49*, 17–36.

Maniak, M. (1999). Endocytic transit in *Dictyostelium*. Protoplasma *210*, 25–30.

Maniak, M. (2001). Fluid-phase uptake and transit in axenic *Dictyostelium* cells. Biochim. Biophys. Acta *1525*, 197–204.

Maniak, M., Rauchenberger, R., Albrecht, R., Murphy, J., and Gerisch, G. (1995). Coronin involved in phagocytosis: dynamics of particle-induced relocalization visualized by a green fluorescent protein tag. Cell *83*, 915–924.

Marsh, M., G. Griffiths, G. Dean, I. Mellman, and H.A. (1986). Three-dimensional structure of endosomes in BHK-21 cells. Proc. Natl. Acad. Sci. USA *83*, 2899–2903.

Matteoni, R., and Kreis, T.E. (1987). Translocation and clustering of endosomes and lysosomes depends on microtubules. J. Cell Biol. *105*, 1253–1265.

McCaffrey, G., and Vale, R.D. (1989). Identification of a kinesin-like microtubule based motor protein in *Dictyostelium discoideum*. EMBO J. *8*, 3229–3234.

McDowall, A., Gruenberg, J., Romisch, K., and Griffiths, G. (1989). The structure of organelles of the endocytic pathway in hydrated cryosections of cultured cells. Eur. J. Cell Biol. *49*, 281–94.

Mellman, I. (1996). Endocytosis and molecular sorting. Annu. Rev. Cell Dev. Biol. *12*, 575–625.

Monaghan, P., and Robertson, D. (1990). Freeze-substitution without aldehyde or osmium fixatives: ultrastructure and implications for immunocytochemistry. J. Microsc. *158*, 355–363.

Munn, A. (2001). Molecular requirements for the internalization step of endocytosis: insights from yeast. Biochim. Biophys. Acta *1535*, 236–257.

Neuhaus, E.M., Horstmann, H., Almers, W., Maniak, M., and Soldati, T. (1998). Ethane-freezing/methanol-fixation of cell monolayers. A procedure for improved preservation of structure and antigenicity for light and electron microscopies. J. Struct. Biol. *121*, 326–342.

Neuhaus, E.M., and Soldati, T. (1999). Molecular mechanisms of membrane trafficking. What do we learn from *D. discoideum*? Protist *150*, 235–243.

Neuhaus, E.M., and Soldati, T. (2000). A myosin I is involved in membrane recycling from early endosomes. J. Cell Biol. *150*, 1013–1026.

Nolta, K.V., Rodriguez-Paris, J.M., and Steck, T.L. (1994). Analysis of successive endocytic compartments isolated from *Dictyostelium discoideum* by magnetic fractionation. Biochim. Biophys. Acta *1224*, 237–246.

O'Halloran, T.J., and Anderson, R.G. (1992). Clathrin heavy chain is required for pinocytosis, the presence of large vacuoles, and development in *Dictyostelium*. J. Cell Biol. *118*, 1371–1377.

Padh, H., Ha, J., Lavasa, M., and Steck, T.L. (1993). A post-lysosomal compartment in *Dictyostelium discoideum*. J. Biol. Chem. *268*, 6742–6747.

Parton, R.G., Joggerst, B., and Simons, K. (1994). Regulated internalization of caveolae. J. Cell Biol. *127*, 1199–1215.

Pollock, N., de Hostos, E.L., Turck, C.W., and Vale, R.D. (1999). Reconstitution of membrane transport powered by a novel dimeric kinesin motor of the Unc104/KIF1A family purified from *Dictyostelium*. J. Cell Biol. *147*, 493–505.

Pollock, N., Koonce, M.P., de Hostos, E.L., and Vale, R.D. (1998). In vitro microtubule-based organelle transport in wild-type *Dictyostelium* and cells overexpressing a truncated dynein heavy chain. Cell Motil. Cytoskeleton *40*, 304–314.

Prescianotto-Baschong, C., and Riezman, H. (1998). Morphology of the yeast endocytic pathway. Mol. Biol. Cell *9*, 173–189.

Rauchenberger, R., Hacker, U., Murphy, J., Niewohner, J., and Maniak, M. (1997). Coronin and vacuolin identify consecutive stages of a late, actin-coated endocytic compartment in *Dictyostelium*. Curr. Biol. *7*, 215–218.

Riezman, H., Munn, A., Geli, M.I., and Hicke, L. (1996). Actin-, myosin- and ubiquitin-dependent endocytosis. Experientia.*52*, 1033–1041.

Roberts, R.L., Barbieri, M.A., Pryse, K.M., Chua, M., Morisaki, J.H., and Stahl, P.D. (1999). Endosome fusion in living cells overexpressing GFP-Rab5. J. Cell Sci. *112*, 3667–3675.

Roos, U.P., de Brabander, M., and Nuydens, R. (1987). Movements of intracellular particles in undifferentiated amebae of *Dictyostelium discoideum*. Cell Motil. Cytoskeleton *7*, 258–271.

Rupper, A., and Cardelli, J. (2001). Regulation of phagocytosis and endo-phagosomal trafficking pathways in *Dictyostelium discoideum*. Biochim. Biophys. Acta *1525*, 205–216.

Ruscetti, T., Cardelli, J.A., Niswonger, M.L., and O'Halloran, T.J. (1994). Clathrin heavy chain functions in sorting and secretion of lysosomal enzymes in *Dictyostelium discoideum*. J. Cell Biol. *126*, 343–352.

Ryter, A., and de Chastellier, C. (1977). Morphometric and cytochemical studies of *Dictyostelium discoideum* in vegetative phase. Digestive system and membrane turnover. J. Cell Biol. *75*, 200–217.

Scepek, S., and Lindau, M. (1993). Focal exocytosis by eosinophils–compound exocytosis and cumulative fusion. EMBO J. *12*, 1811–1817.

Schroer, T.A. (2000). Motors, clutches and brakes for membrane traffic. Traffic *1*, 3–10.

Schwarz, E., Neuhaus, E.M., Kistler, C., Henkel, A., and Soldati, T. (2000). *Dictyostelium* myosin IK is involved in the maintenance of cortical tension and affects motility and phagocytosis. J. Cell Sci. *113*, 621–633.

Slot, J.W., and Geuze, H.J. (1985). A new method of preparing gold probes for multiple-labeling cytochemistry. Eur. J. Cell Biol. *38*, 87–93.

Smart, E.J., Foster, D., Ying, Y.S., Kamen, B.A., and Anderson, R.W.G. (1993). Protein kinase C activators inhibit recepto-mediated potocytosis by preventing internalization of caveolae. J. Cell Biol. *124*, 307–313.

Souza, G.M., Mehta, D.P., Lammertz, M., Rodriguez-Paris, J., Wu, R.R., Cardelli, J.A., and Freeze, H.H. (1997). *Dictyostelium* lysosomal proteins with different sugar modifications sort to functionally distinct compartments. J. Cell Sci. *110*, 2239–2248.

Steyer, J.A., and Almers, W. (1999). Tracking single secretory granules in live chromaffin cells by evanescent-field fluorescence microscopy. Biophys. J. *76*, 2262–2271.

Steyer, J.A., and Almers, W. (2001). A real-time view of life within 100 nm of the plasma membrane. Nat. Rev. Mol. Cell. Biol. *2*, 268–275.

Steyer, J.A., Horstmann, H., and Almers, W. (1997). Transport, docking and exocytosis of single secretory granules in live chromaffine cells. Nature *388*, 474–478.

Stout, A.L., and Axelrod, D. (1989). Evanescent field excitation of fluorescence by epi-illumination microscopy. Appl. Opt. *28*, 5237–5242.

Sussman, M. (1987). Cultivation and synchronous morphogenesis of *Dictyostelium* under controlled experimental conditions. Methods Cell Biol. *28*, 9–29.

Swanson, J., Bushnell, A., and Silverstein, S.C. (1987). Tubular lysosome morphology and distribution within macrophages depend on

integrity of cytoplasmic microtubules. Proc. Natl. Acad. Sci. USA *84*, 1921–1925.

Swanson, J.A., Johnson, M.T., Beningo, K., Post, P., Mooseker, M., and Araki, N. (1999). A contractile activity that closes phagosomes in macrophages. J. Cell Sci. *112*, 307–316.

Thilo, L. (1985). Quantification of endocytosis-derived membrane traffic. Biochim. Biophys. Acta *822*, 243–266.

Toomre, D., Steyer, J.A., Keller, P., Almers, W., and Simons, K. (2000). Fusion of constitutive membrane traffic with the cell surface observed by evanescent wave microscopy. J. Cell Biol. *149*, 33–40.

Tooze, J., and Hollinshead, M. (1991). Tubular early endosomal network in AtT20 and other cells. J. Cell Biol. *115*, 635–653.

van Deurs, B., von Bulow, F., Vilhardt, F., Holm, P.K., and Sandvig, K. (1996). Destabilization of plasma membrane structure by prevention of actin polymerization. Microtubule-dependent tubulation of the plasma membrane. J. Cell Sci. *109*, 1655–1665.

Wall, D.A., Wilson, G., and Hubbard, A.L. (1980). The galactose-specific recognition system of mammalian liver: the route of ligand internalization in rat hepatocytes. Cell *21*, 79–93.

Wendland, B., McCaffery, J.M., Xiao, Q., and Emr, S.D. (1996). A novel fluorescence-activated cell sorter-based screen for yeast endocytosis mutants identifies a yeast homologue of mammalian eps15. J. Cell Biol. *135*, 1485–1500.

Willingham, M.C., and Yamada, S.S. (1978). A mechanism for the destruction of pinosomes in cultured fibroblasts: piranhalysis. J. Cell Biol. *78*, 480–487.

Xiao, Z., and Devreotes, P.N. (1997). Identification of detergent-resistant plasma membrane microdomains in *Dictyostelium*: enrichment of signal transduction proteins. Mol. Biol. Cell *8*, 855–869.

Zhu, Q., and Clarke, M. (1992). Association of calmodulin and unconventional myosin with the contractile vacuole complex of *Dictyostelium discoideum*. J. Cell Biol. *118*, 347–358.